13
Opportunities in Nanotechnology via Organic Solid-state Reactivity: Nanostructured Co-crystals and Molecular Capsules

Dejan-Krešimir Bučar, Tamara D. Hamilton, and Leonard R. MacGillivray

13.1
Introduction

Organic reactions are generally carried out in solution (i.e. liquid phase) [1]. However, a variety of organic reactions (e.g. oxidation, elimination, photoreactions) occur in the solid state, providing regio- and enantioselective access to molecular products in high yields [2]. Photoinduced solid-state reactions [3] were discovered at the beginning of the last century. In the early 1900s, Riiber discovered that cinnamylidineacetic acid and cinnamylidinemalonic acid photodimerize to give cyclobutanes upon UV irradiation [4]. Two decades later, Stobbe's and de Jong's groups discovered that different polymorphs of cinnamic acid yield two different photoproducts upon UV irradiation [5]. This surprising observation was attributed to crystal-packing effects of cinnamic acid molecules in the different polymorphs. The mechanistic details of such solid-state reactions were, at that point, not well understood, but their intriguing nature provoked further studies to elucidate mechanisms.

In the 1960s, Schmidt accomplished crystallographic and photochemical studies of a wide range of cinnamic acids. Schmidt recognized the structural requirements for [2 + 2] photodimerizations to proceed in the solid state. Schmidt proposed that two C=C bonds should be aligned parallel and separated by <4.2 Å to react [6]. These requirements are known as the topochemical postulates. Although the topochemical postulates are extremely valuable for predicting whether a photodimerization will occur, frustrating effects of close packing [7] have largely thwarted efforts to synthesize molecules in solids using the carbon–carbon (C−C) bond-forming reaction with synthetic freedoms (e.g. control of product size) experienced in solution.

13.2
Template-controlled [2 + 2] Photodimerization in the Solid State

In recent years, we have introduced a method to control [2 + 2] photodimerizations in the solid state using molecular templates [8]. We have employed this method as a

Organic Nanostructures. Edited by Jerry L. Atwood and Jonathan W. Steed

ISBN: 978-3-527-31836-0

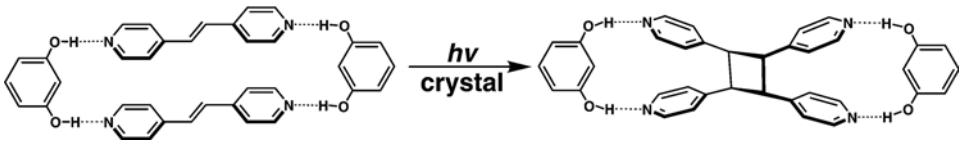

Scheme 13.1

means to circumvent the effects of close packing [7]. We have shown that ditopic molecules (e.g. resorcinol, 1,8-naphthalenedicarboxylic acid), in the form of linear templates, can preorganize olefins in positions suitable for the photoreaction. The templates organize the olefins via hydrogen bonds into positions largely independent of long-range packing (Scheme 13.1). Thus, we have shown that co-crystallization of resorcinol (res) with *trans*-1,2-bis(4-pyridyl)ethylene (4,4′-bpe) produces a discrete, four-component hydrogen-bonded assembly, 2(res)·2(4,4′-bpe), in which two C=C bonds are arranged for a [2 + 2] photodimerization (Figure 13.1a). UV irradiation of the solid produced *rctt*-1,2,3,4-tetrakis(4-pyridyl)cyclobutane (4,4′-tpcb) (where *rctt* reference,*cis*,*trans*,*trans*) stereospecifically and in 100% yield (Figure 13.1b) [8]. The photoproduct was isolated via basic extraction. Later, we showed that that this supramolecular approach to control solid-state reactivity is tolerant to molecular size by enabling the construction of complex molecular targets (e.g. ladderanes) [9].

Having developed a means to achieve control of the [2 + 2] photodimerization in the solid state, we now discuss, in this chapter, how the field of solid-state reactivity provides opportunities for emerging studies in the area of nanotechnology. In

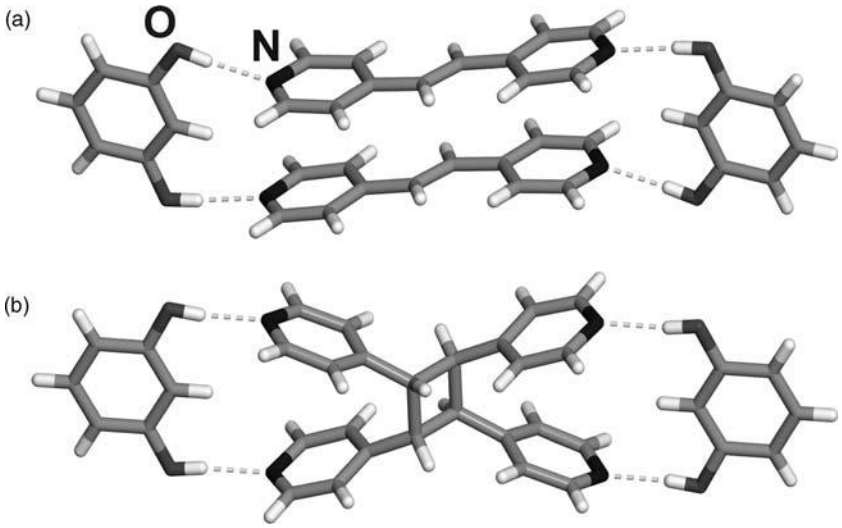

Figure 13.1 X-ray crystal structures of (a) 2(res)·2(4,4′-bpe) and (b) 2(res)·2(4,4′-tpcb).

particular, we will first describe how the template approach has led us to a method that facilitates the construction of nanostructured organic co-crystals using sonochemistry [10]. We will show how sonocrystallization produces nanostructured co-crystals that exhibit a rare phenomenon known as single crystal-to-single crystal (SCSC) reactivity. Second, we will demonstrate how the photoproducts of the template method can be used, *following the solid-state syntheses*, as organic building units of self-assembled molecular capsules [11,12].

13.3
Nanostructured Co-crystals

Upon UV irradiation of crystalline (res)·2(4,4′-bpe), each C-atom of the C=C bond of the olefin undergoes a change in position to form the cyclobutane ring. Such movement is invariably accompanied by the accumulation of strain and stress in the solid [13]. The accumulation of strain and stress can, and most often does, result in a collapse of the crystal lattice. The collapse will cause the single crystals to turn opaque and crack. We determined that macrosized single crystals of (res)·2(4,4′-bpe) crack upon photoreaction (Figure 13.2) [10]. Examples of solid-state reactions in which the integrity of single crystals remain virtually unchanged are rare. In such an SCSC reaction [13], the product forms homogeneously within the solid phase of the reactant.

SCSC reactions are intriguing to study for two general reasons [13]. First, SCSC reactions provide an ability to study reaction mechanisms and pathways by monitoring a reaction via single-crystal X-ray diffraction. Second, such solids have potential to be incorporated into solid-state devices (e.g. ultra-high-density data storage). The rareness of SCSC reactivity combined with the promise in materials science has created a need to generate materials that undergo SCSC reactions by design. Approaches to achieve SCSC reactivity of the [2 + 2] photodimerization have involved either adjusting the UV source for tail-end absorption of the reactant or, as will be discussed in more detail here, the use of crystals of nanometer-scale dimensions [13a].

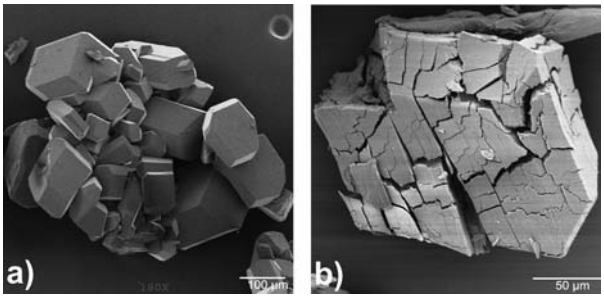

Figure 13.2 SEM micrographs of macro-sized co-crystals of (res)·2(4,4′-bpe) (a) before and (b) after photoreaction. Adapted from Ref. [10] with permission from the American Chemical Society.

In our laboratory, we have used the tail-end UV absorption method to achieve SCSC reactivity within our templated solids. We have shown, for example, that SCSC reactivity can be achieved with 2-(1,8-naphthalenedicarboxylic acid)·2(3,4′-bpe) [14]. Studies on similar template-based co-crystals, however, have demonstrated that the tail-end method does not ensure SCSC reactivity [10]. To circumvent this problem, we aimed to achieve SCSC reactivity using co-crystals of nanometer-scale dimensions.

13.3.1 Organic Nanocrystals and Single Crystal-to-single Crystal Reactivity

Organic nanocrystals have attracted much attention owing to potential applications in electronics, biotechnology and catalysis [15–20]. The increasing interest in the properties of organic nanocrystals has led to numerous methods to synthesize such materials (e.g. sonication, microemulsion, vapor condensation). In this context, Nakanishi and coworkers have described a method to fabricate organic nanocrystals under relatively mild conditions. The method is based on reprecipitating an organic molecule during a solvent-exchange process [21–25]. They also demonstrated that the [2 + 2] photodimerization can proceed in an SCSC fashion by reducing the crystal size to nanometer-scale dimensions [26]. In particular, pure diolefin crystals of nano- and micrometer dimensions were fabricated via the reprecipitation method. The single crystals were shown to generate a polycyclobutane through an SCSC transformation. Macroscopic single crystals of the diolefin failed to undergo SCSC reaction and collapsed during the photoreaction. From these studies, we anticipated that an SCSC [2 + 2] photoreaction involving our photoactive co-crystals could be achieved by decreasing the crystal size to nanometer-scale dimensions.

Our first experiment to prepare nanometer-sized co-crystals of 2(res)·2(4,4′-bpe) using the reprecipitation method did not succeed [10]. In particular, an ethanolic solution of res and 4,4′-bpe was injected into water and vigorously stirred. As expected, the ethanolic solution created a cloudy suspension owing to precipitation of 2(res)·2(4,4′-bpe), which is poorly soluble in water. SEM images revealed particles of primarily micrometer dimensions (i.e. $>5\,\mu m$). The majority of the particles were non-uniform in shape and exhibited uneven edges and irregular, flake-like morphologies (Figure 13.3a). The formation of the particles was attributed to an inherent mismatch in the solubilities of the molecular components of the co-crystal. UV irradiation resulted in cracking and destruction of the crystalline solids (Figure 13.3b).

To overcome the limitations of the reprecipitation method, we turned to sonocrystallization [27]. In particular, we combined low-intensity ultrasonic radiation using a water-bath with reprecipitation to synthesize nano- and micrometer-sized co-crystals of 2(res)·2(4,4′-bpe) [10]. In a typical experiment, ultrasonic radiation was immediately applied to a cloudy low-temperature (approximately 10 °C) suspension of res, 4,4′-bpe, ethanol and water obtained after concomitant addition of ethanol solutions of res and 4,4′-bpe into water using a microsyringe. SEM images revealed the formation of well-defined crystals of uniform shape and a size distribution [28] of 500 nm–8 μm (Figure 13.4a). Upon UV irradiation, single crystals of 2(res)·2(4,4′tpcb)

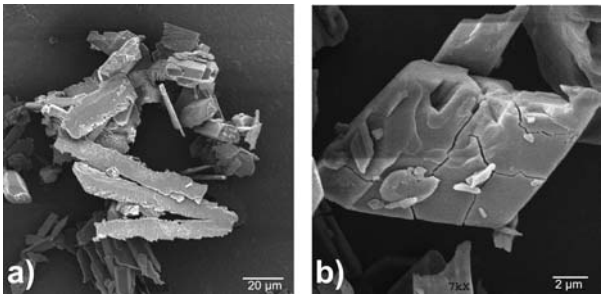

Figure 13.3 SEM images of co-crystals of (res)·2(4,4′-bpe) via the reprecipitation method (a) before and (b) after photoreaction. Adapted from Ref. [10] with permission from the American Chemical Society.

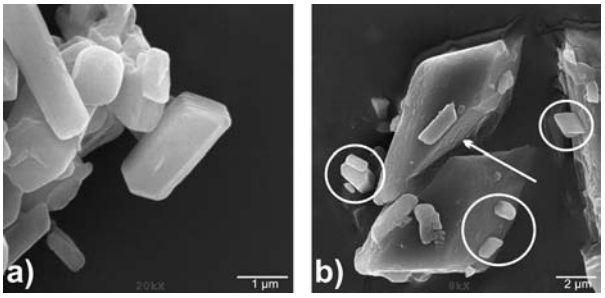

Figure 13.4 SEM images of nanostructured (res)·2(4,4′-bpe) (a) before and (b) after photoreaction. Arrows show cracks in large macrocrystals and circles show intact co-crystals. Adapted from Ref. [10] with permission from the American Chemical Society.

of less than 2 µm underwent an SCSC transformation, whereas the larger macrosized crystals cracked (Figure 13.4b). We attributed the formation of the nanostructured co-crystals of 2(res)·2(4,4′-bpe) to effects of cavitation. The process is associated with high temperatures (i.e. up to 5000 °C) and pressures (i.e. 1000 atm), which result in the formation, growth and rapid collapse of bubbles in a liquid environment [29]. Moreover, we attributed the generation of the nanostructured materials to cavitation being able to rapidly solubilize the components of 2(res)·2(4,4′-bpe) [30] and, at the same time, provide a mechanism for fast precipitation and formation of the solids.

13.4
Self-assembled Capsules Based on Ligands from the Solid State

In recent years, widespread attention has been devoted to self-assembled metal–organic frameworks with structures that conform to polygons and polyhedra [31]. The internal cavities of such discrete frameworks are studied for applications in areas

such as logic gates, nano-sized reaction vessels and delivery systems [31]. We have shown that the photoproducts of template-controlled reactions in the solid state can be used to generate metal–organic polygons and polyhedra [11,12]. We determined that *rctt*-1,2-bis(2-pyridyl)-3,4-bis(4-pyridyl)cyclobutane (2,4′-tpcb) can be an organic connector of both a polygon [11a] and polyhedron [11b]. We have also shown that *rctt*-1,2-bis(2-pyridyl)-3,4-bis(3-pyridyl)cyclobutane (2,3′-tpcb) can act as a connector of a polyhedron [11c]. It is instructive to note that Nature employs a conceptually similar approach to construct polyhedral hosts (i.e. viruses). Specifically, the linear structure of deoxyribonucleic acid (DNA) directs the formation of organic subunits (i.e. proteins) that, in a second step, form a functional, self-assembled structure [32]. For 2,4′-tpcb and 2,3′-tpcb, each cyclobutane possessed a chelating unit based on the 2-pyridyl group and two monodentate units based on either the 4- or 3-pyridyl group (Figure 13.5). Both cyclobutanes were synthesized in the solid state using a resorcinol stereospecifically, in quantitative yield and gram amounts [11].

Our first report described the ability of 2,4′-tpcb to self-assemble with Cu(II) ions to form a hexanuclear polyhedron in form a trigonal antiprism in $[Cu_6(2,4\text{-tpcb})_6(H_2O)_6][ClO_4]_{12}$ (Figure 13.6). The hexanuclear assembly, $[Cu_6(2,4\text{-tpcb})_6(H_2O)_6]^{12+}$, formed upon reaction of 2,4′-tpcb and $Cu(ClO_4)_2{\cdot}6H_2O$ [11a]. The six Cu(II) ions occupied the vertices of the antiprism. Each Cu(II) ion was coordinated by a 2-pyridyl chelating unit, two 4-pyridyl monodentate units and a water molecule to form a nearly square-prism coordination environment. Consequently, the 4-pyridyl groups corresponded to the edges of the antiprism and the 2-pyridyl groups corresponded to the corners. As a result of the assembly process, a cylindrical cavity that encapsulated two ClO_4^- anions formed.

We also determined that 2,4′-tpcb serves as a building unit of a metal-organic polygon. Reaction of copper(II) hexafluoroacetylacetonate (hfac) with 2,4′-tpcb

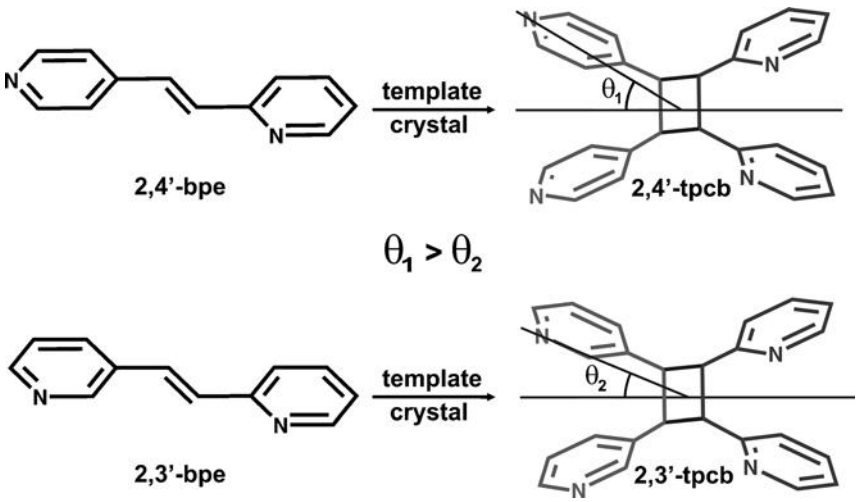

Figure 13.5 Polydentate ligands derived from the solid state that support metal–organic polygons and polyhedra: (a) 2,3′-tpcb and (b) 2,4′-tpcb.

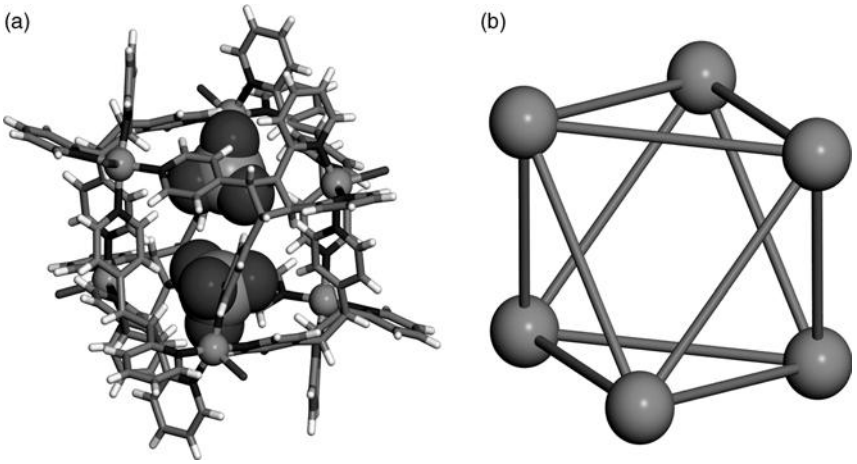

Figure 13.6 X-ray structure of $[Cu_6(2,4\text{-tpcb})_6(H_2O)_6]^{12+}$: (a) encapsulated ClO_4^- ions and (b) topology of the trigonal antiprism based on the Cu(II) ions (Cu(II) ions are displayed using the ball-and-stick model and the ClO_4^- ions using the space-fill model).

produced a tetranuclear metal–organic polygon $[Cu_4(2,4'\text{-tpcb})_2(hfac)_8]$, with a geometry that conformed to a rhombus (Figure 13.7). In contrast to the polyhedron, each metal atom adopted an octahedral coordination environment. The 4-pyridyl groups provided the edges of the polygon. The cavity of the polygon was too small to accommodate an organic molecule as a guest. This was the first example in which an organic connector unit supported the structures of both and polyhedron and polygon [32].

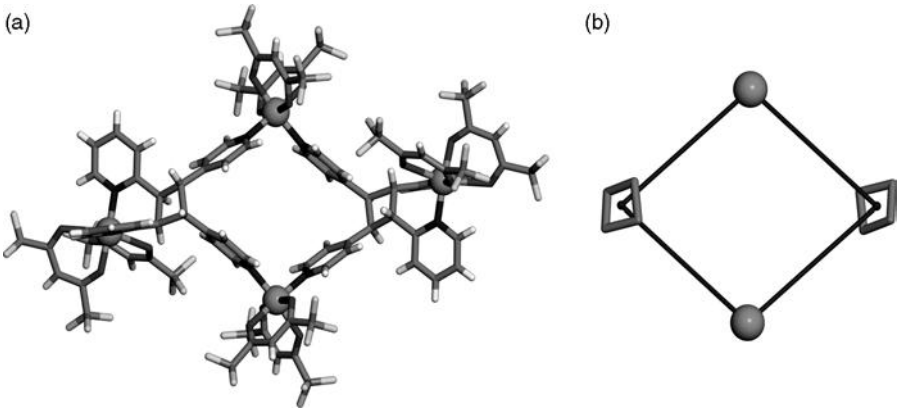

Figure 13.7 X-ray structure of $[Cu_4(2,4\text{-tpcb})_2(hfac)_8]$: (a) stick view and (b) topology of the polygon based on the Cu(II) ions and cyclobutane rings [Cu(II) ions are displayed using the ball-and-stick model].

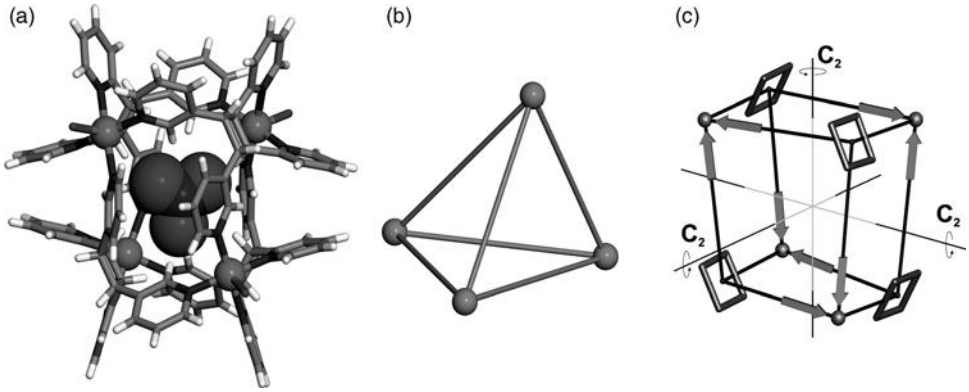

Figure 13.8 X-ray crystal structure of $[Cu_4(2,3'\text{-tpcb})_4(H_2O)_4]^{8+}$ showing: (a) encapsulated NO_3^- ion, (b) topology of the tetrahedron based on the Cu(II) ions and (c) placement of the Cu(II) ions and cyclobutane rings showing how the directionality of the 3-pyridyl groups precludes mirror symmetry [Cu(II) ions are displayed using the ball-and-stick model and the NO_3^- ions using the space-fill model].

To build on our observation involving the polyhedron $[Cu_6(2,4\text{-tpcb})_6(H_2O)_6]^{12+}$, we anticipated that a second polyhedron could form using the related isomer 2,3′-tpcb. We expected that the exchange of the 4-pyridyl group with a 3-pyridyl group would produce a smaller polyhedron owing to a decrease in the angle of the coordination-vector (Figure 13.5). Reaction of 2,3′-tpcb with Cu(II) ions afforded the tetranuclear polyhedron $[Cu_4(2,3'\text{-tpcb})_4(H_2O)_4]^{8+}$ with a structure that conformed to a tetrahedron (Figure 13.8) [11c]. As expected, the polyhedron based on 2,3′-tpcb was smaller than that based on 2,4′-tpcb, with the inner cavity hosting only a single NO_3^- ion as a guest. To our surprise, however, the tetrahedron exhibited a chiral topology [12]. The polyhedron displayed approximate D_2 symmetry. The chirality was a result of the geometric fit of the metal and organic components along the surface of the capsule. As with the trigonal antiprism, the Cu(II) ions occupied the vertices of the tetrahedron. Each Cu(II) ion adopted an approximately square pyramidal coordination environment.

13.5 Summary and Outlook

In this chapter, we have described a method to direct reactivity in the organic solid state using molecular templates. We have shown how nanostructured co-crystals of the template-based materials can be synthesized using sonochemistry. We have also shown how the nanostructured solids support SCSC reactivity involving the [2 + 2] photodimerization. The use of sonochemistry overcomes difficulties of controlled nucleation and crystal growth, presumably caused by mismatching of the solubilities of the components of a co-crystal. We have also demonstrated how the molecules

synthesized using templates in the solid state can be used as organic building blocks of self-assembled capsules. The method has provided a route to molecular capsules akin to the approach employed by Nature. Collectively, the studies involving the nanostructured co-crystals and the molecular capsules provide opportunities for studies in nanotechnology via templated reactions directed in organic solids.

References

1 Smith, M.B. and March, J. (2007) in *March's Advanced Organic Chemistry: Reactions, Mechanisms and Structure*, Wiley, Hoboken, NJ.

2 (a) Kaupp, G. (2005) Organic Solid-State. Reactions with 100% Yield. *Top. Curr. Chem.*, **254**, 95–183. (b) Tanaka, K. and Toda, F. (2000) Solvent-Free Organic Syntheses. *Chem. Rev.*, **100**, 1025–1074.

3 Ramamurthy, V. and Venkatesan, K. (1987) Photochemical Reactions of Organic Crystals. *Chem. Rev.*, **87**, 433–481.

4 (a) Riiber, C.N. (1902) Die Synthese der α-Truxillsäure. *Chem. Ber.*, **35**, 2411–2415. (b) Riiber, C.N. (1913) Die Licht-Polymerisation der Cinnamyliden-essigsäure. *Chem. Ber.*, **46**, 335–338.

5 (a) Stobbe, H. and Steinberger, F.K. (1922) Lichtreaktionen der *trans*-und *cis*-Zimtsäuren. *Chem. Ber.*, **55B**, 2225–2245. (b) Stobbe,H. and Lehfeldt, A. (1925) Polymerisationen und Depolymerisationen durch Licht verschiedener Wellenlänge, II.: α- und β-*trans*-Zimtsäure, allo-Zimtsäure und ihre Dimeren. *Chem. Ber.*, **58B**, 2415–2427. (c) de Jong, A.W.K. (1923) Über die Konstitution der Truxill- und Truxinsäuren und über die Einwirkung des Sonnenlichtes auf die Zimtsäuren und Zimtsäure-Salze. *Chem. Ber.*, **56B**, 818–832. (d) de Jong, A.W.K. (1922) Über die Einwirkung des Lichtes auf die Zimtsäuren und über die Konstitution der Truxillsäuren. *Chem. Ber.*, **55B**, 463–474.

6 Schmidt, G.M.J. (1971) Photodimerization in the Solid State. *Pure Appl. Chem.*, **27**, 647–678.

7 Desiraju, G.R. (1995) Supramolecular Synthons in Crystal Engineering – A New Organic Synthesis. *Angew. Chem. Int. Ed.*, **34**, 2311–2327.

8 MacGillivray, L.R., Reid, J.L. and Ripmeester, J.A. (2000) Supramolecular Control of Reactivity in the Solid State Using Linear Molecular Templates. *J. Am. Chem. Soc.*, **122**, 7817–7818.

9 Gao, X., Friscic, T. and MacGillivray, L.R. (2004) Supramolecular Construction of Molecular Ladders in the Solid State. *Angew. Chem. Int. Ed.*, **43**, 232–236.

10 Bučar, D..-K. and MacGillivray, L.R. (2007) Preparation and Reactivity of Nanocrystalline Co-Crystals Formed via Sonocrystallization. *J. Am. Chem. Soc.*, **129**, 32–33.

11 (a) Hamilton, T.D., Papaefstathiou, G.S. and MacGillivray, L.R. (2002) A Polyhedral Host Constructed Using a Linear Template. *J. Am. Chem. Soc.*, **124**, 11606–11607. (b) Papaefstathiou, G.S., Hamilton, T.D. and MacGillivray, L.R. (2004) Self-Assembled Metal–Organic Squares Derived from Linear Templates as Exemplified by a Polydentate Ligand that Provides Access to Both a Polygon and Polyhedron. *Chem. Commun.*, 270–271. (c) Hamilton, T.D., Bučar, D..-K. and MacGillivray, L.R. (2007) Coding a Coordination-Driven Self-Assembly via a Hydrogen-Bond-Directed Solid-State Synthesis: an Unexpected Chiral Tetrahedral Capsule. *Chem. Commun.*, 1603–1604.

12 Hamilton, T.D. and MacGillivray, L.R. (2004) Enclosed Chiral Environments from Self-Assembled Metal–Organic Polyhedra. *Cryst. Growth Des.*, **4**, 419–430.

13 (a) Friščić, T. and MacGillivray, L.R. (2005) Single-Crystal-to-Single-Crystal Transformations Based on the [2+2] Photodimerization: from Discovery to Design. *Z. Kristallogr.*, **220**, 351–363. (b) Halder, G.J. and Kepert, C.J. (2006) Single Crystal to Single Crystal Structural Transformations in Molecular Framework Materials. *Aust. J. Chem.*, **59**, 597–604.

14 Varshney, D.B., Papaefstathiou, G.S. and MacGillivray, L.R. (2002) Site-Directed Regiocontrolled Synthesis of a "Head-to-Head" Photodimer via a Single-Crystal-to-Single-Crystal Transformation Involving a Linear Template. *Chem. Commun.*, 1964–1965.

15 Zhao, Y.S., Yang, W. and Yao, J. (2006) Organic Nanocrystals with Tunable Morphologies and Optical Properties Prepared Through a Sonication Technique. *Phys. Chem. Chem. Phys.*, **8**, 3300–3303.

16 Jang, J. and Oh, J.H. (2003) Facile Fabrication of Photochromic Dye-Conducting Polymer Core-Shell Nanomaterials and Their Photoluminescence. *Adv. Mater.*, **15**, 977–980.

17 Kwon, E., Oikawa, H., Kasai, H. and Nakanishi, H. (2007) A Fabrication Method of Organic Nanocrystals Using Stabilizer-Free Emulsion. *Cryst. Growth Des.*, **7**, 600–602.

18 Zhao, Y.S., Yang, W., Xiao, D., Sheng, X., Yang, X., Shuai, Z., Luo, Y. and Yao, J. (2005) Single Crystalline Submicrotubes from Small Organic Molecules. *Chem. Mater*, **17**, 6430–6435.

19 Chiu, J.J., Kei, C.C., Perng, T.P. and Wang, W.S. (2003) Organic Semiconductor Nanowires for Field Emission. *Adv. Mater.*, **15**, 1361–1364.

20 Masuhara, H., Nakanishi, H. and Sasaki, K. (eds)(2003) *Single Organic Nanoparticles*, Springer, Berlin.

21 Kasai, H., Nalwa, H.S., Oikawa, H., Okada, S., Matsuda, H., Minami, N., Kakuta, A., Ono, K., Mukoh, A. and Nakanishi, H. (1992) A Novel Preparation Method of Organic Microcrystals. *Jpn. J. Appl. Phys.*, **31**, L1132–L1134.

22 Kasai, H., Oikawa, H., Okada, S. and Nakanishi, H. (1998) Crystal Growth of Perylene Microcrystals in the Reprecipitation Method. *Bull. Chem. Soc. Jpn.*, **71**, 2597–2601.

23 Baba, K., Kasai, H., Okada, S., Oikawa, H. and Nakanishi, H. (2000) Novel Fabrication Process of Organic Microcrystals using Microwave Irradiation. *Jpn. J. Appl. Phys.*, **39**, L1256–L1258.

24 Nakanishi, H. and Kasai, H. (1997) Polydiacetylene Microcrystals for Third-Order Nonlinear Optics. *ACS Symp. Ser.*, **672**, 183–198.

25 Chung, H.-R., Kwon, E., Oikawa, H., Kasai, H. and Nakanishi, H. (2006) Effects of Solvent on Organic Nanocrystal Growth Using the Reprecipitation Method. *J. Cryst. Growth*, **294**, 459–463.

26 Takahashi, S., Miura, H., Kasai, H., Okada, S., Oikawa, H. and Nakanishi, H. (2002) *J. Am. Chem. Soc.*, **124**, 10944–10945.

27 (a) Bang, J.H. and Suslick, K.S. (2007) Sonochemical Synthesis of Nanosized Hollow Hematite. *J. Am. Chem. Soc.*, **129**, 2242–2243. (b) Dhas, N.A. and Suslick, K.S. (2005) Sonochemical Preparation of Hollow Nanospheres and Hollow Nanocrystals. *J. Am. Chem. Soc.*, **127**, 2368–2369.

28 Veerman, M., Resendiz, M.J.E. and Garcia-Garibay, M. (2006) Large-Scale Photochemical Reactions of Nanocrystalline Suspensions: a Promising Green Chemistry Method. *Org. Lett.*, **8**, 2615–2617.

29 (a) Suslick, K.S. (1990) *Sonochemistry. Science*, **247**, 1439–1445. (b) Suslick, K.S. and Price, G.J. (1999) Applications of Ultrasound to Materials Chemistry. *Annu. Rev. Mater. Sci.*, **29**, 295–326.

30 Ruecroft, G., Hipkiss, D., Ly, T., Maxted, N. and Cains, P.W. (2005) Sonocrystallization: the Use of Ultrasound for Improved Industrial Crystallization. *Org. Process Res. Dev.*, **9**, 923–932.

31 (a) Seidel, S.R. and Stang, P.J. (2002) High-Symmetry Coordination Cages via Self-Assembly. *Acc. Chem. Res.*, **35**, 972–983. (b) Gianneschi, N.C., Masar, M.S., III. and Mirkin, C.A. (2005) Development of a Coordination Chemistry-Based Approach for Functional Supramolecular Structures. *Acc. Chem. Res.*, **38**, 825–837. (c) Caulder, D.L. and Raymond, K.N. (1999) Supermolecules by Design. *Acc. Chem. Res.*, **32**, 975–982.

32 Hamilton, T.D., Papaefstathiou, G.S. and MacGillivray, L.R. (2005) Template-Controlled Reactivity: Following Nature's Way to Design and Construct Metal–Organic Polygons and Polyhedra. *J. Solid State Chem.*, **178**, 2409–2413.

14
Organic Nanocapsules

Scott J. Dalgarno, Nicholas P. Power, and Jerry L. Atwood

14.1
Introduction

By exploiting the principles of supramolecular chemistry, nature has mastered the ability to form remarkably complex molecular capsules on a widely varied scale. This chapter is focused on reviewing the principles upon which molecular capsules are constructed at all length scales. Research in our group has involved: (1) the synthesis of new building blocks for capsules; (2) the engineering of functionality into such capsules; (3) the extension of length scales from the nano- to the micro-level, providing robust capsules; and (4) the understanding of the structural relationship of spheres (capsules) to tubes. Success in these endeavors will afford nanocpasules for applications in drug delivery and catalysis. The increased understanding of the principles governing the assembly of larger capsules will provide insight into aspects of living systems.

Dimeric capsules held together by covalent bonds were prepared in the 1980s by Collet [1] and Cram et al. [2], and self-assembled dimeric capsules were reported by Conn and Rebek [3] and others [4–8] in the 1990s. Dimeric capsules generally possess an internal volume in the range 100–300 $Å^3$. Monomeric capsules have also been characterized [9]. In this chapter, we will summarize the development of larger capsules, capsules which may be measured on the nano-length scale, capsules possessing an internal volume exceeding 800 $Å^3$.

14.2
First Generation Nanocapsules

In 1997, we discovered a spherical assembly consisting of [(*C*-methylresorcin[4]arene)$_6$(H_2O)$_8$], **1**. This assembly (Figure 14.1), with an enclosed volume of 1375 $Å^3$, was characterized by a single-crystal X-ray diffraction study and was found to be stable in non-polar solvents [10]. The evidence that **1** maintains the capsule structure in

Organic Nanostructures. Edited by Jerry L. Atwood and Jonathan W. Steed

ISBN: 978-3-527-31836-0

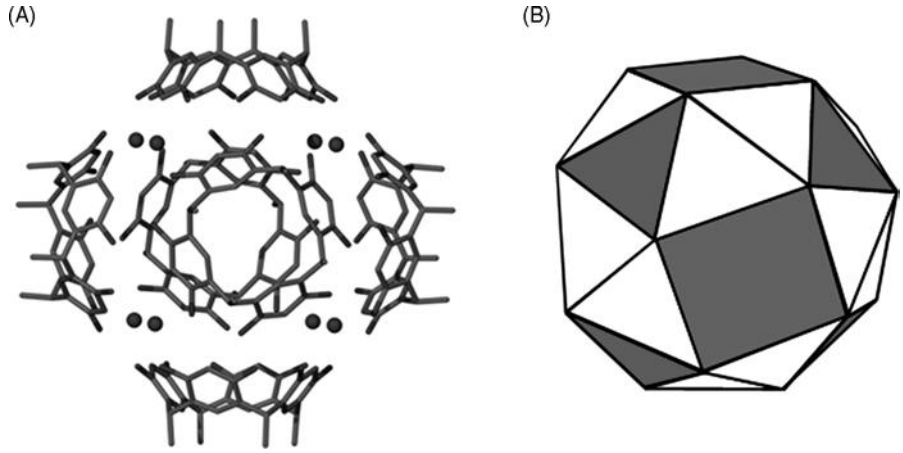

Figure 14.1 (A) The near-spherical nanocapsule assembly, **1**, based on *C*-methylresorcin[4]arene and water, formed from wet nitrobenzene [10]. The capsule is composed of six resorcin[4] arenes and eight structural water molecules. (B) The hydrogen bonding pattern representing the Archimedean solid, the *snub cube*.

solution was obtained from both one- and two-dimensional ^{1}H NMR studies. The spectrum of **1** in benzene-d_6 at increasing concentrations shows resonances attributed to the chiral and achiral calixarenes as well as the eight water molecules. These observations, coupled with the molecular mass determination in benzene (7066 g mol^{-1}), [11], provide convincing evidence supporting the nanocapsule structure of **1** in solution. Many subsequent studies have supported this initial conclusion of solution stability for the nanocapsule [12,13].

We were also able to link the geometry of the nanocapsule **1** to the Archimedean solid known as the *snub cube* (Figure 14.1B). In a review, we have set forth structural classifications and general principles for the design of nanocapsules based, in part, on the solid geometry ideas of Plato and Archimedes [14]. Indeed, we have used the well-known solid geometry principles embodied in Platonic and Archimedean solids to design new, large spherical container assemblies. A recent success involved the construction and characterization of an *icosahedron* made up of *p*-sufonatocalix[4] arenes, pyridine *N*-oxide, metal ions and water [15].

The discovery of the link between the solid geometry principles of Plato and Archimedes and the chemical assembly of small building blocks into large supramolecular structures was important. Specifically, the discovery that members of the resorcin[4]arene family self-assemble to form the capsule shown as **1** in Figure 14.1 prompted our research group to examine the topologies of related spherical hosts with a view to understanding their structures on the basis of symmetry. In addition to providing a basis for classification, it was anticipated that such an approach would allow one to identify similarities at the structural level, which, at the chemical level, may not seem obvious and may be used to design large, spherical host assemblies similar to **1**.

Our group has now described the results of this analysis which we regard as the development of a general strategy for the construction of spherical molecular hosts. In these reports we began by presenting the idea of self-assembly in the context of spherical hosts and then, after summarizing the Platonic and Archimedean solids, we provided examples of cubic symmetry-based hosts, from both the laboratory and nature, with structures that conform to these polyhedra.

To construct a spherical host from two subunits ($n = 2$), each unit must cover half of the sufrace of the sphere. This can only be achieved if the subunits exhibit cruvature and they are placed such that their centroids lie at a maximum distance from each other. These criteria place two points along the surface of a sphere separated by a distance equal to the diameter of the shell. As a consequence of this arrangement, there exist two structure types: one with two identical subunits attached at the equator and one belonging to the point group D_{nd} which is topologically equivalent to a tennis ball.

To construct a spherical host from three subunits ($n = 3$), each must cover one-third of the surface of the sphere. Following the design conditions described previously, placing three identical subunits along the surface of a sphere results in an arrangement in which their centroids constitute the vertices of an equilateral triangle. As a result, there is only one structure type, that belonging to D_{3h}. Each of the subunits must exhibit curvature.

For $n = 4$, positioning four points along the surface of a sphere such that they lie a maximum distance from each other places the points at the vertices of a tetrahedron. This is the first case in which joining the points via line segments gives rise to a closed surface container. The container, a tetrahedron, is comprised of four identical subunits, in the form of equilateral triangles where surface curvature is supplied by edge-sharing of regular polygons rather than by the subunits themselves.

The Platonic solids comprise a family of five convex uniform polyhedra which possess cubic symmetry and are made of the same regular polygons (equilateral triangle, square, pentagon) arranged in space such that the vertices, edges and three coordinate directions of each solid are equivalent. That there is a finite number of such polyhedra is due to the fact that there exists a limited nuber of ways in which identical regular polygons may be adjoined to construct a convex corner. There are thus only five such isometric polyhedra, all of which are achiral.

In addition to the Platonic solids, there exists a family of 13 convex uniform polyhedra known as the Archimedean solids. Each member of this family is made up of at least two different regular polygons and may be derived from at least one Platonic solid through either truncation or twisting of faces. In the case of the latter, two chiral members, the *snub cube* and the *snub dodecahedron*, are realized. The remaining Archimedean solids are achiral.

It is important to realize the limitations of the Platonic and Archimedean solid models for supramolecular assemblies. For the *snub dodecahedron*, a total of 60 triangles are called for, but triangles can be simply the result of hydrogen bonds from adjacent triangles or pentagons. For example, the *snub cube* in Figure 14.1 is composed of 32 triangles and six squares, with the triangles being represented by water molecules and the squares, resorcin[4]arenes. However, in nanocapsule **1** only

eight of the 32 triangles contain water molecules, as one can observe from the shading. Therefore, in the search for the *snub dodecahedron*, the ratio of water to calix[5]arene pentacarboxylic acid cannot be higher than 60:12 and it is likely to be lower.

14.3 Second Generation Nanocapsules

In the theme of control of the guest species by external forces, a discovery was made which relates to the *p*-sulfonatocalix[4]arene capsules first reported in 1999 [15]. In the solid state, truncated cone-shaped *p*-sulfonatocalix[4]arene, **2**, favors the formation of infinite bilayer structures in which neighboring calixarenes are orientated in an up–down fashion relative to one another (Figure 14.2) [16]. However, it is possible to circumvent the formation of such bilayer structures under controlled conditions for a ternary system containing pyridine *N*-oxide (PNO), a lanthanide(III) nitrate salt and the pentasodium salt of *p*-sulfonatocalix[4]arene, Na_5**2** (Figure 14.3) [15].

Parallel (up–up) packing of neighboring calixarenes imparts significant curvature to the overall assembly, resulting in the formation of either spheroidal or tubular arrays. The spheroidal array consists of 12 calixarenes arranged at the vertexes of an icosahedron (Figure 14.3). Indeed, this is the most symmetrical way in which to arrange 12 like objects efficiently about a Platonic/Archimedean solid. The calixarenes enclose a central core comprised of two sodium ions and 30 water molecules that form an extensively hydrogen-bonded regime within the capsule [15]. Since icosahedra are unable to pack closely in three dimensions by sharing vertexes, edges or faces, the near spheroids do not form a close-packed arrangement in the extended solid. The spheroidal structure is based on a C-shaped dimer, consisting of two molecules of **2** linked to a common trivalent lanthanide ion by way of metal–sulfonate coordination. Furthermore, each of the calixarene cavities contains a PNO molecule, which is also coordinated to the bridging lanthanide ion. Each component of the dimer forms part of a separate spheroid and neighboring superstructures can therefore be considered to be multiply bridged by means of first and second sphere coordination of lanthanide ions.

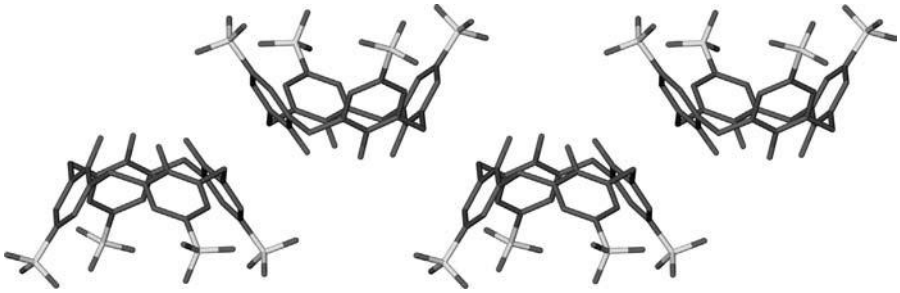

Figure 14.2 Schematic of *p*-sulfonatocalix[4]arene, **2**, and an example of a favorable bilayer anti-parallel arrangement found in the solid state [16].

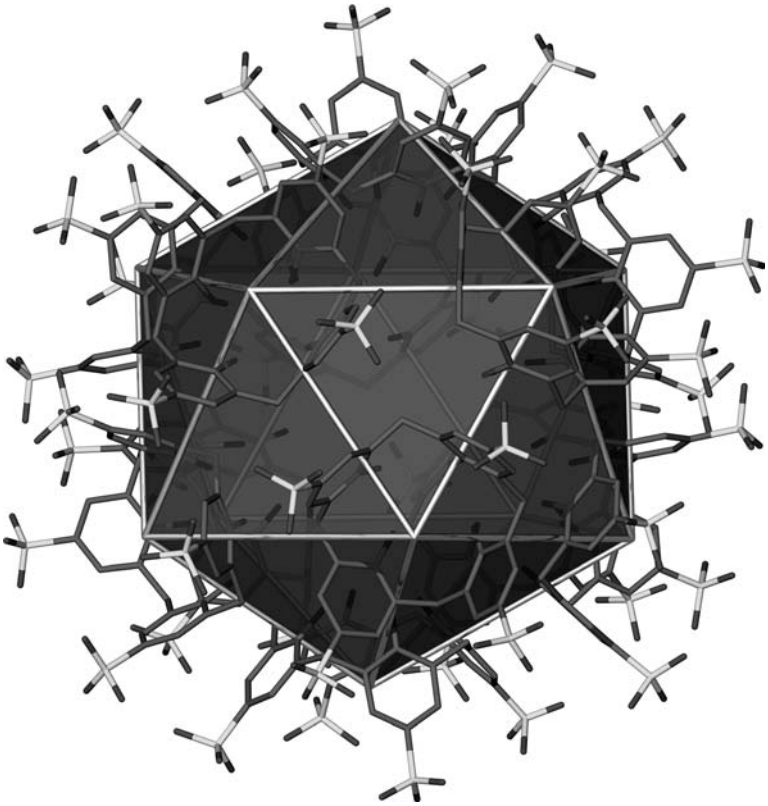

Figure 14.3 Arrangement of 12 *p*-sulfonatocalix[4]arene molecules at the vertexes of an icosahedron to form a compact spherical assembly [15].

We have now shown that replacement of PNO by 18-crown-6 in the above-mentioned ternary system results in a remarkably dissimilar spheroidal array consisting of 12 calixarenes arranged at the vertexes of a cuboctahedron (Figure 14.4) [17,18]. We attribute the formation of this new type of spheroid to the constraint placed upon facing calixarenes of neighboring spheres by their shared 18-crown-6 guests. The relative rigidity of the shared crown ether guest forces facing calixarenes of the {**2**–crown ether–**2**} dimer to be eclipsed relative to one another, whereas the {**2**–PNO–lanthanide–PNO–**2**} dimer is bridged by multisphere coordination (as the C-shaped dimer). We believe that a discrete spheroidal entity comprising 12 molecules of **2** would favor placement of the components at the vertexes of an icosahedron, since this arrangement is the most compact of the 12-vertex Platonic and Archimedean solids. However, when the spheres are arranged to form a three-dimensional solid, either cubic or hexagonal close-packed arrangements of the multicomponent entities should be favored. Therefore, we understand that the extended structure has arranged itself such that the spheres are situated along vectors representing the vertexes of either a cuboctahedron (Archimedean solid,

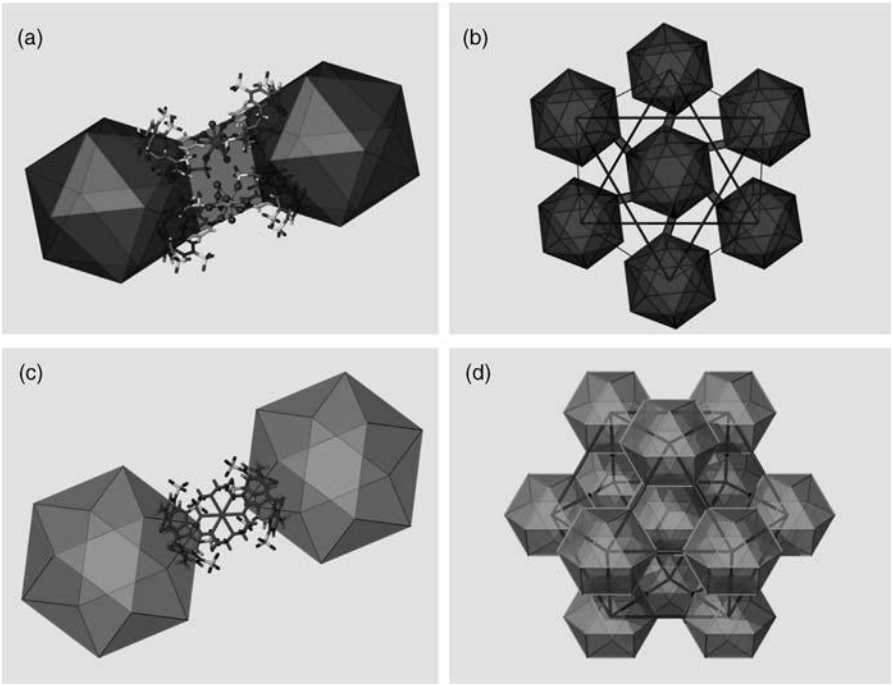

Figure 14.4 Guests external to the 12-calixarene assemblies based on **2** determine the packing and symmetry of the capsule [17,18]. (a) Icosahedral nanocapsules linked by C-shaped dimers. (b) Packing of icosahedra in an anti-prismatic fashion. (c) Linking of cuboctahedral arrays by {**2**–crown ether–**2**} linkages. (d) Cubic close packing of neighboring cuboctahedra.

cubic close-packed) or a triangular orthobicupola (Johnson solid capable of hexagonal close packing by vertex–vertex alignment).

The internal volume of the icosahedral arrangement is calculated to be 975 $Å^3$, whereas the cuboctahderal geometry (Figure 14.4) contains a volume of 1260 $Å^3$. This represents an increase of about 30% in enclosed volume upon reorganization from icosahedral to cuboctaheral packing. This disparate packing of calixarenes has a dramatic effect on both the chemical composition and nature of the outer shell. The calixarenes are arranged such that the shell of each sphere contains six pores in which disordered water molecules are situated. These pores have a van der Waals diameter of 4.2 Å and are arranged at the vertexes of an octahedron centered at the core of the capsule. This arrangement can be thought of as a channel for the communication of molecular material between the hydrophilic interior of the capsule, through the hydrophobic shell, to the hydrophilic exterior [17,18]. The amount of 'chemical space' enclosed by either of the two capsules is about 1000 $Å^3$. As discussed above, this space (in the icosahedral case) houses 30 water molecules and two sodium ions. However, the van der Waals volume of these capsules is about 11 000 $Å^3$ (this calculation is based on the approximate nanocapsule diameter). The second generation capsules

are differentiated from **1**, the first generation capsules, by several factors. First, the supramolecular forces used to hold together capsule **1** together are hydrogen bonds, while a combination of van der Waals forces, π-stacking interactions and metal ion coordinate covalent bonds is employed for the *p*-sulfonatocalix[4]arenes of the second generation. Second, the surface which encloses the chemical space is essentially one atom thick for **1**, while it is the thickness of the *p*-sulfonatocalix[4]arene building block in the second generation nanocapsules (hence the 11 000 $Å^3$ volume of the assembly with only 1000 $Å^3$ of space within). Third, the contents of the capsule are rather completely ordered for the second generation capsules (by the hydrogen bonds from the enclosed water to the phenolic oxygen atom hydrogen bond acceptors at the base of the *p*-sulfonatocalix[4]arene), but the contents are completely disordered for **1** (because of the lack of any directional bonding force connecting the skeleton of the assembly to the contents therein).

An important outgrowth of the work described above was the discovery of a method of control of molecular architecture such that in one example a spherical assembly (an *icosahedron*, a Platonic solid) was converted into a tubular structure [15]. This will be discussed along with other similar examples at the end of the chapter. It is important to emphasize that the second generation nanocapsule can be formed from a wide range of metal ions, both 3+ (lanthanides) and 2+ (cadmium), and the stoichiometry of the reaction mixture controls the architecture of the final product, sphere or tubule.

14.4
Third Generation Nanocapsules

In 1999 there was a report [19] of a large supramolecular assembly related to our resorcin[4]arene work. The synthesis of *C*-isobutylpyrogallol[4]arene (Figure 14.5A), **3**, was accomplished under mild conditions [19]. However, the authors reported that

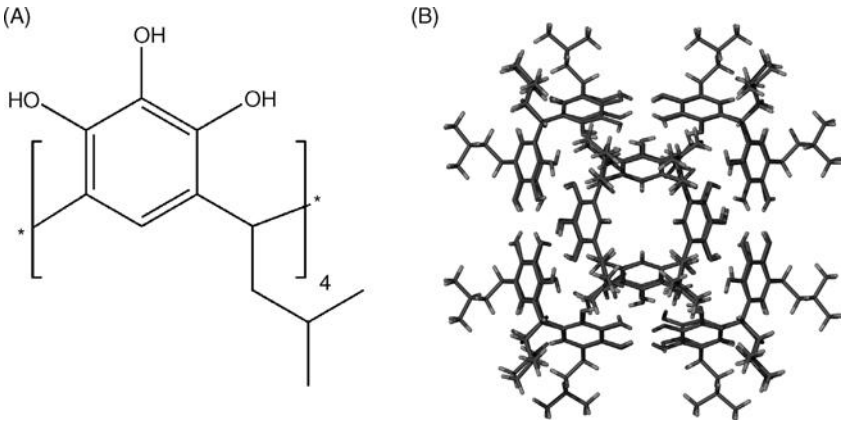

Figure 14.5 (A) Schematic of *C*-isobutylpyrogallol[4]arene. (B) Self-assembled capsule of *C*-isobutylpyrogallol[4]arene, as crystallized from acetonitrile [19].

they obtained the self-assembled hexamer of **3** only one time out of many attempts (Figure 14.5B). Further, this lack of reproducibility was used as evidence that the hexamer is unstable compared with our [(*C*-methylresorcin[4]arene)$_6$(H_2O)$_8$], **1** [10]. This did not seem credible, since the hexamer appears to be held together by 72 hydrogen bonds, 48 of which are intermolecular. This means that the assembly is bound together by eight intermolecular hydrogen bonds per bonded entity. Capsule **1** is bound together by 36 intermolecular hydrogen bonds or 2.6 per bonded molecule. For comparsion, the tennis ball of Rebek's group [20] is bound together by four hydrogen bonds per bonded molecule. It seemed to us that the pyrogallol[4]arene hexamer should be more, not less, stable than our [(*C*-methylresorcin-[4]arene)$_6$ (H_2O)$_8$] capsule in the same solvents.

We therefore synthesized a variety of pyrogallol[4]arenes by the acid-catalyzed condensation of pyrogallol with appropriate aldehydes [21–23]. The yields are high, approaching quantitative, and although pyrogallol[4]arenes can often be crystallized in bilayer motifs [24], we obtained X-ray structural data for the hexamer **3** with R = ethyl, propyl, isobutyl, butyl, hexyl and others. The hexamer for R = butyl is shown in Figure 14.6 and the formation of this nanocapsule is fairly reproducible [24]. We have obtained various hexamer from a variety of solvents, including Et_2O

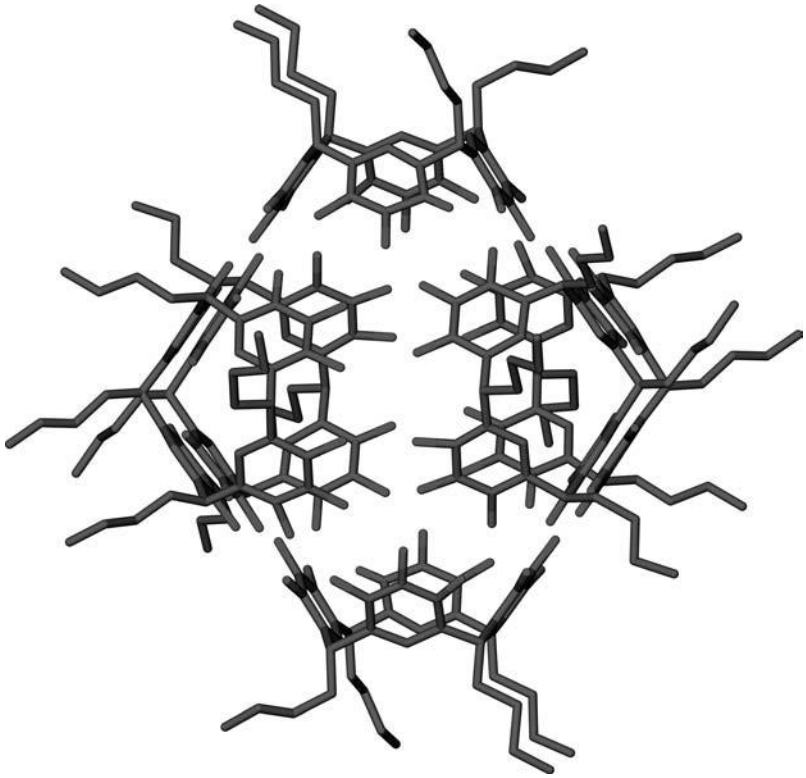

Figure 14.6 Structure of the hexameric *C*-butylpyrogallol[4]arene nanocapsule [24].

with nitrobenzene and, surprisingly, methanol. We have also studied these pyrogallol [4]arenes by NMR techniques in a variety of solvents in order to assess their stability and their binding properties (as have others) [25–27]. The volume available for guests is $\sim$1500 Å^3, so the range of guests available for study is vast [25].

In a preliminary test of the stability of the *C*-isobutylpyrogallol[4]arene hexamer, crystals of the compound were slurried in water and sonicated for 30 min. The solid was then collected on a frit and dried under vacuum. The powder pattern of the compound after the water treatment was the same as that before the treatment (in each case, the characteristic low angle peak of the hexamer was observed). The *C*-isobutylpyrogallol[4]arene hexamer is insoluble in water and the water does not degrade the spherical structure.

A key feature of biological systems is the encapsulation of entities within a structure. A spherical virus is a beautifully complex example of this enclosure of chemical space [28]. Until now, such biological capsules have been beyond the synthetic grasp of the chemist because of the vast size and complexity of the enclosure. A further complication which has not often been addressed in the chemical literature of cell mimics is the very high level of organization found on the interior of enclosures of biological importance.

Indeed, once the enclosure of space has been accomplished, the organization of the guests contained within becomes a key issue. Rebek and coworkers have used steric constraints to organize two guests within a tubular dimer [29], but for those assemblies with large enclosed volumes, both discrete and infinite, the guests are most often disordered [14,17–19,21–24]. The one example of significant order within such an enclosure is the polar core consisting of 30 water molecules and two sodium ions in the second generation 12-*p*-sulfonatocalix[4]arene assembly [15].

In the first structurally authenticated hexamers (generally represented by **3**), it was not possible to determine any geometric information relating to the included guest molecules. We have subsequently shown that the guest molecules trapped within the host container may adjust their spatial orientation in response to interactions between adjacent nanocapsules. Remarkably, functionalizing the outer shell of the nanocapsule with different alkyl chains leads to highly specific solid-state packing arrangements, which in turn influence the organization of the guest molecules within the capsules. In the course of this work, it was discovered that the nanocapsules may be synthesized reproducibly in quantitative yields under normal laboratory conditions by crystallization from ethyl acetate [21]. TG–IR analysis of the R = heptyl capsules revealed that ethyl acetate molecules are released from the crystalline material at two distinct stages during gradual heating of a dried sample: a weight loss of 7.5% (70–105 °C) corresponds to the loss of only the six ethyl acetate molecules external to the cavity; a further weight loss of 8% immediately prior to decomposition (225–275 °C) corresponds to the loss of both bound ethyl acetate and water molecules from the cavity. In comparison, TG–IR analysis of the monomer rather than the capsule shows no significant weight loss above the boiling point of the solvent, until rapid decomposition occurs at 290 °C. Consistent with the TG–IR studies, the crystal structure of the R = heptyl capsule shows that six ethyl acetate molecules enshroud a disordered water molecule within the host assembly.

With respect to crystal packing, the cases when R = pentyl and heptyl afford simple hexagonal and hexagonal-closest packing arrays, respectively, with capsules separated by their lipophilic tails. However, for R = hexyl the nanocapsules are not forced away from one another by the hexyl tails, but rather congregate to form hydrogen-bonded nanorods (Figure 14.7). Four OH groups on opposite sides of each capsule form hydrogen bonds with two adjacent capsules. Consequently, the walls of the individual nanocapsules are disrupted, which translates through to the packing of the guest species within the capsule.

The distorted intermolecular hydrogen bonding within the host walls enables four of the ethyl acetate guest molecules to undergo hydrogen bonding to the nanocapsule wall through their carbonyl functionalities. The nanocapsules for R = pentyl and heptyl feature ordered arrays of ethyl acetate molecules enshrouding a water molecule [21]. The methyl groups are orientated towards the base of the pyrogallol[4]arene macrocycles and the single water molecule resides at the center of the enclosed space. When the neighboring nanocapsules communicate with each other through the hydrogen bonding interactions observed in the R = hexyl nanocapsule (Figure 14.7), the four ethyl acetate guest molecules hydrogen bonded to the inside of the nanocapsule wall reorient with their ethyl groups in the base of the macrocycle (Figure 14.8). The two remaining ethyl acetate guests position their methyl groups down into the cleft of the macrocycle. It was not possible to locate the exact position of the water molecule inside the nanocapsules owing to extensive disorder. However, the difference in guest interactions is clearly a consequence of communication or lack thereof between the host walls of neighboring nanocapsules. This initial result opens the way to control guest orientation by forces external to the capsules.

In an extension to this work, we have been examining the encapsulation of probe molecules in these large assemblies with a view to reporting on the nature of the "inner phase" of these large assemblies [30–34]. We found that sonication of a hot saturated acetonitrile solution of *C*-hexylpyrogallol[4]arene and excess pyrenebutyric acid (PBA) [30] afforded dark single crystals (crystals of solvent containing capsules are colorless) [24] that were studied using X-ray crystallography. These studies showed the capsule to encase two pyrene butyric acid molecules that were "bound"

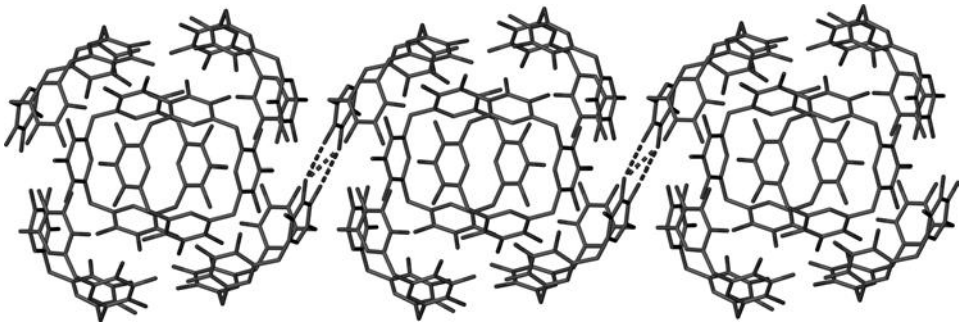

Figure 14.7 Some of the hydrogen bonding interactions found between nanocapsule walls when *C*-hexylpyrogallol[4]arene is crystallized from ethyl acetate [21].

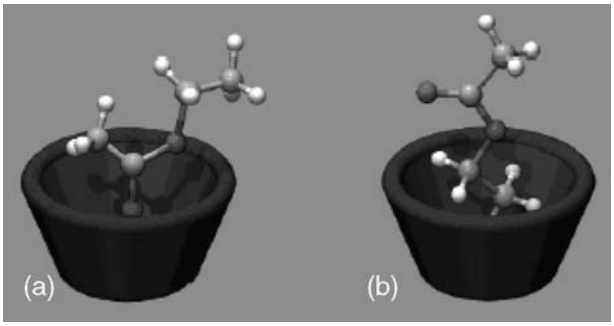

Figure 14.8 Guest molecules within nanocapsules orient differently depending on the environment external to the overall assembly [21]. In (a) the methyl group of the ethyl acetate is inserted into the pyrogallol[4]arene cavity, whereas in (b) the orientation is reversed, with methyl group insertion observed.

to the capsule wall by π-stacking and CH···π interactions (Figure 14.9). In order to examine whether the assembly was stable in solution, single crystals were dissolved in a non-polar medium (hexane) and the stability of the assembly was followed by spectrofluorimetry in the presence of an appropriate quencher (dimethylaniline). Unfortunately, it was not possible to deconvolute fully the interactions between the

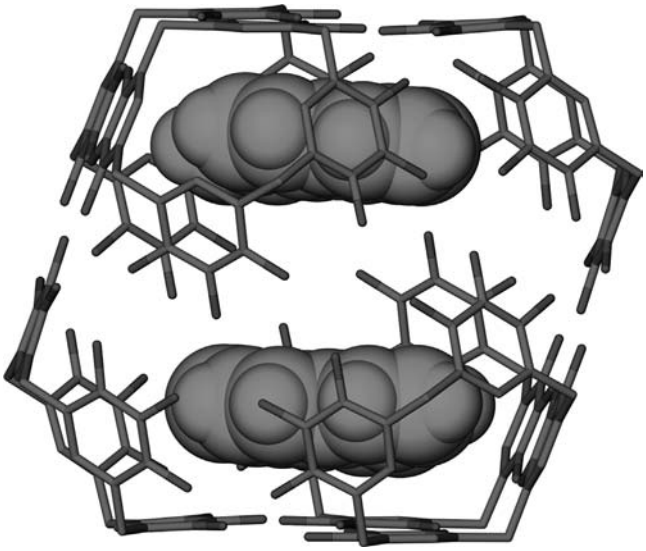

Figure 14.9 Part of the single crystal X-ray structure of the *C*-hexylpyrogallol[4]arene hexameric nanocapsule shrouding two pyrene butyric acid molecules [30]. The guests are found to stick to the wall through π-stacking and CH···π interactions and are well separated (by around 8 Å) by the butyric acid side-chains and co-encapsulated acetonitrile molecules.

butyric acid functionality of the PBA and the capsule seam hydroxyl groups due to extensive disorder within the large assembly. This was also impeded by the fact that single crystals of these materials are typically small and weakly diffracting. However, both analytical techniques support the retention of the guest-containing assembly and other polyaromatic probes were examined for similar behavior. Perylene, benzo [*a*]pyrene and pentacene have also been successfully encapsulated, although without appropriate side-chain functionality it appears that these probes are not retained even in non-polar media [31]. This feature may also be responsible for lower capsule population that precludes structural characterization due to weak diffraction and high levels of disorder. Through computational studies on a "half-capsule" in the presence of a guest, we believe these guest species to be too large to form the favorable interactions described above for PBA and initial spectrofluorimetry studies appear to show that the probes are rapidly released upon crystal dissolution [32]. In this regard,

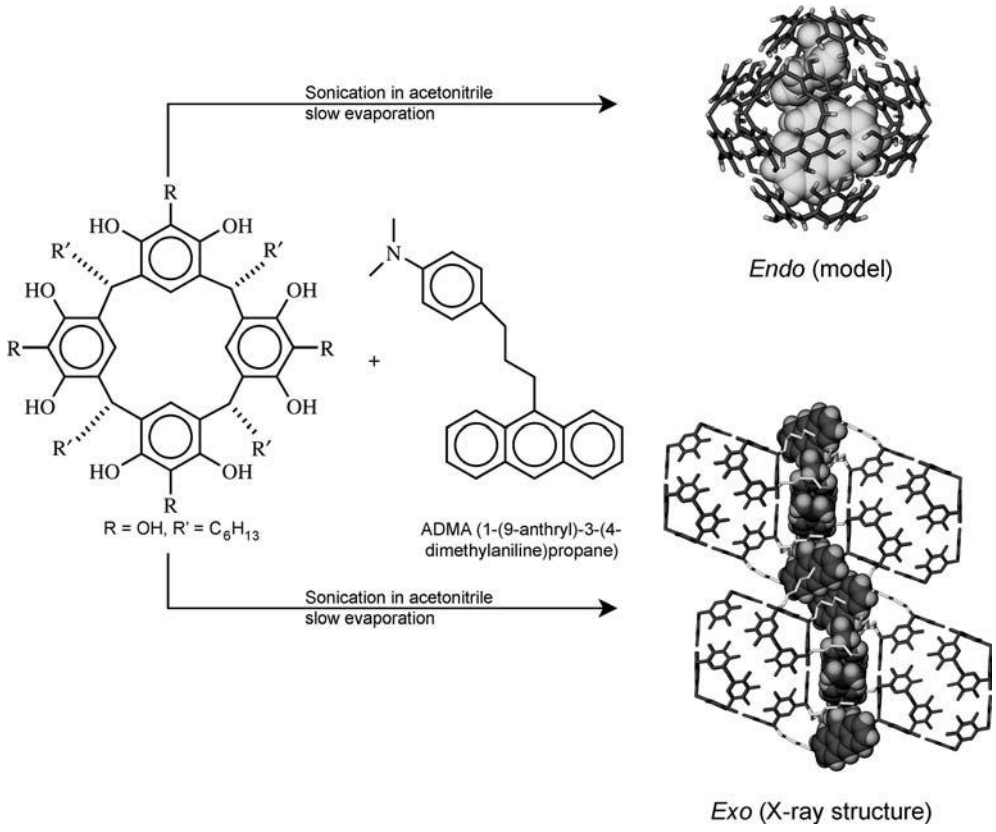

Figure 14.10 Schematic of the formation of *C*-hexylpyrogallol[4]arene assemblies with the probe ADMA residing either *endo* and *exo* to the nanocapsule motif [33,34]. In the *exo* case, the probe forms channels within the structure, pushing neighboring nanocapsules apart.

we are currently exploring the side-chain functionality as a method of capsule stabilization.

When a probe incorporating a "built-in" quencher, 4-[3-(9-anthryl)propyl]-*N*,*N*-dimethylaniline (ADMA), was employed, two very different situations arose with respect to guest interaction with the pyrogallol[4]arene nanocapsules [33,34]. In the majority of cases it was possible to obtain crystals of the probe-containing capsules, but on rare occasions it was possible to obtain crystals of different morphology, all of which were studied using single-crystal X-ray crystallography. The inner phase of the capsule-containing probes was not determinable, which is likely due to the reasons outlined above, but for the different morphology crystals the probe was found to reside *exo* to the capsule and was also found to push the capsules apart through the formation of channels of ADMA in the solid state (Figure 14.10) [33]. Both assemblies were followed by spectrofluorimetry [in tetrahydrofuran (THF)], showing distinctively different spectra. In order to determine whether aggregates of the *exo* probe structure were present in the solution phase, the solution was sonicated to release the guest from the arrangement, producing a characteristic spectrum of the free probe in THF. Various other probe molecules containing quenchers are also being explored for similar behavior.

14.5
Fourth Generation Nanocapsules

The fourth generation of capsules is somewhat related to the previously reported capsule formulated as [(*C*-methylresorcin[4]arene)$_6$(H_2O)$_8$]. Capsule **1** possesses an excess of four hydrogen bond donors, but these donors are positioned such that they project outward from the surface of the enclosure [10]. In this orientation they are incapable of effecting organization of the guests within the capsule. In a similar fashion, all the hydrogen bond donors in [(pyrogallol[4]arene)$_6$] are typically used in completing the hydrogen bond pattern that forms the capsule; the guests within are generally not ordered, except in those cases described above for third generation capsules [21]. It was reasoned that a number of mixed systems consisting of different ratios of pyrogallol and resorcinol subunits might form a capsule (or different capsules) with the desired property of excess of hydrogen bond donors (Figure 14.11). Furthermore, such an asembly may offer the possibility to orient guest species through some of the hydrogen donors that would not be involved in self-complementary hydrogen-bonding. The mixed possibilities are shown as **4**–**7** (Figure 14.11). A modified synthesis of hybrid macrocycle **4** was performed according to the syntheses of resorcin[4]arene and pyrogallol[4]arene and upon recrystallization from diethyl ether (Et_2O), the remarkable structure shown in Figure 14.12 results [35]. The hexamer of **4** takes the shape of a trigonal antiprism with the centers of **4** at the corners of the trigonal antiprism. This assembly, with six hydrogen bond donors positioned toward the interior of the capsule and possesses an internal volume of 860 $Å^3$. The six Et_2O molecules on the interior of the capsule are ordered by six additional hydrogen bond donors. In addition, there are six more hydrogen bond

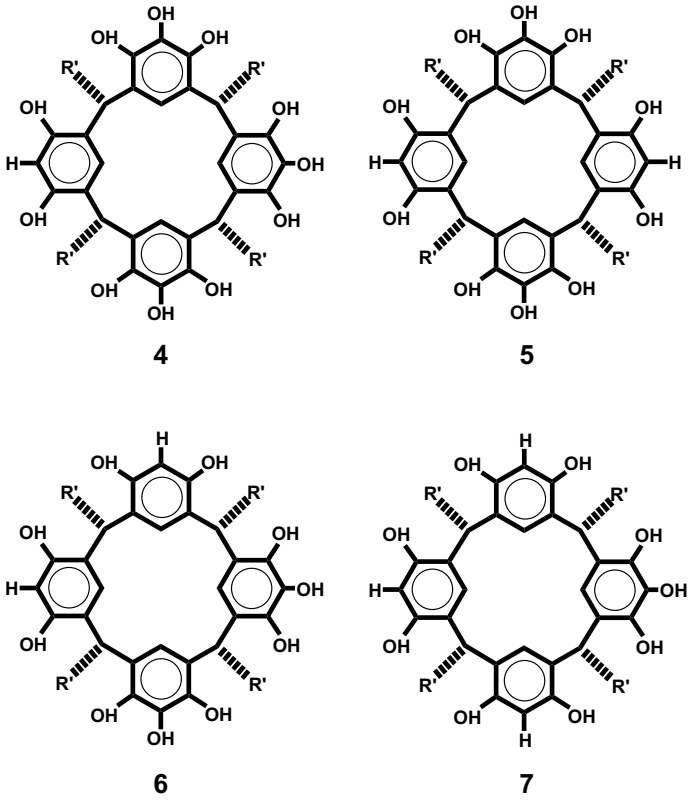

Figure 14.11 Schematic of the mixed resorcinol/pyrogallol[4] arenes formed by performing the literature cyclization in the presence of both subunits [35].

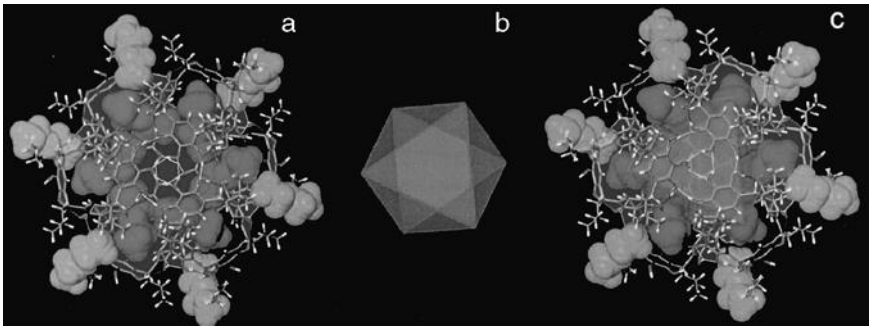

Figure 14.12 The hexameric capsule based on the hybrid macrocycle **4**. (a) The guest diethyl ether molecules and those residing in the shell of the capsule are shown. (b) A trigonal anti-prism. (c) The trigonal anti-prismatic arrangement of guest Et_2O molecules within the capsule and the communication between solvent molecules through the shell [35].

Table 14.1 The mixture of hybrid compounds from the reaction shown in Figure 14.11 [35]. Compounds **3–7** are macrocycles as previously defined. Compounds **8–11** are non-cyclized pyrogallol- and/or resorcinol-containing products.

Compound	%
3	5
4	30
5, **6**	33
7	18
Resorcin[4]arene	3
8	5
9	4
10	3
11	1

donors oriented toward the outside and these donors bind six additional Et_2O molecules on the outside of the hexamer, further sealing the capsule. It is worth noting that there is empty volume at the center of the antiprism. This space is about 80 $Å^3$, enough to accommodate an additional guest of appropriate size and hydrophobicity. However, there is also the possibility that this space could be taken by a larger hydrogen bond-accepting guest; for example, it should be possible to bind five Et_2O and one larger guest.

The mixed macrocycles possess remarkable recognition behaviour. In the initial synthesis of **4**, electrospray mass spectrometry revealed that the first precipitate contains at least 10 different compounds with the macrocycles in approximately the percentages shown in Table 14.1.

By simple probability, it would be unlikely that one would be able to isolate only a single compound from the list in Table 14.1 by crystallization alone. Although this is the case, macrocycle **4** continually crystallizes as a hexameric capsule and therefore must possess enough self-complementarity to afford a mono-composite species. The shape of the resulting capsule is more elliptical when compared with the third generation pyrogallol[4]arene capsules and this is a direct consequence of the hybrid nature of the material and the guest species in the capsule. The pursuit of other capsules from hybrid resorcin/pyrogallol[4]arene monomers is under way, as such assemblies *do* offer directional hydrogen bonding to the capsule interior, a feature we consider important for the future use of such assemblies in areas outlined earlier in the chapter.

14.6 Fifth Generation Nanocapsules

The fifth genearation of capsules is based on hydrogen-bonding templates as theoretical binding sites for metal centers, the idea of which was driven by the

formation of a copper–cyclodextrin complex [36]. In this regard, the hydrogen-bonded hexamer was considered for complexation (or retro-insertion) with copper and gallium centers and the results of these complexation studies are outlined below, with remarkable results.

Initial results were obtained from the combination of *C*-propan-3-olpyrogallol[4]arene with 4 equivalents of $Cu(NO_3)_2$ in an acetone–water solution which gave, on standing, single red crystals of $[Cu_{24}(H_2O)_x(C_{40}H_{40}O_{16})_6(acetone)_n]$ [37]. Characterization by single-crystal X-ray diffraction and MALDI-TOF MS revealed that the metal–organic analogue was a combination of 30 components, where six cavitands had all of their available 48 upper rim phenoxy protons replaced with a concomitant square-planar coordination of 24 Cu^{2+} ions to form 96 new Cu–O bonds and the remaining 24 phenoxy protons involved in intramolecular hydrogen bonding (Figure 14.13).

The distances between the oxygens of the hydrogen-bonded capsule and those of the copper capsule are equitable (differing by only 0.002 Å, Figure 14.13), as are the overall size, shape, symmetry and hence volume for these comparative nanocapsules. This clearly showed that the hydrogen-bonded template as a whole was an excellent example of predicting metal–organic analogues. Although this was the case, we were unable to say whether the metal–organic capsule formation process was due to either a templation effect of the metal centers or perhaps a pre-assembled system prior to metal addition.

Our recent studies in this area have given further insight into the mechanism of formation of these nanocapsules. Reaction of *C*-alkylpyrogallol[4]arenes (C_2–C_{13} alkyl chains) with excess $Cu(NO_3)_2$ in methanol resulted in the instantaneous formation of fine brown precipitates [38]. These precipitates were readily soluble in most organic solvents, however, and it was possible to obtain the single-crystal structure of the *C*-propylpyrogallol[4]arene metal capsule by crystal growth from an acetone solution (although the crystals were weakly diffracting, it was possible to

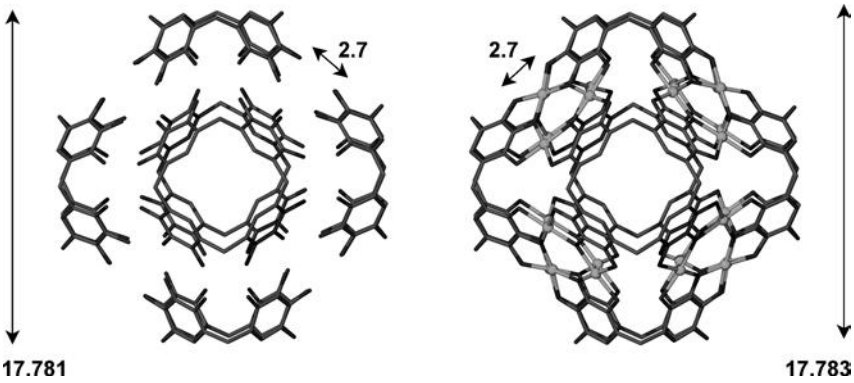

Figure 14.13 Comparison between the hydrogen-bonded (left) and copper bound (right) nanocapsules showing similarities in structure, shape and size of each assembly. Distances shown are in ångstroms [37].

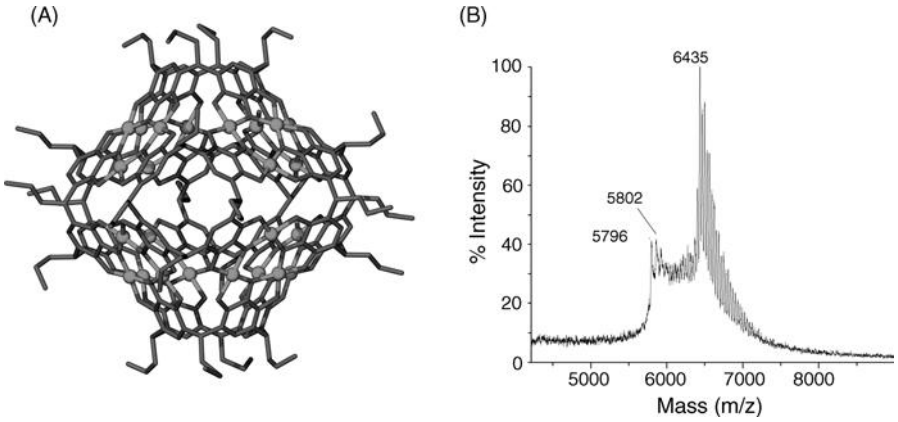

Figure 14.14 (A) Partial crystal structure of the copper *C*-propylpyrogallol[4]arene. (B) MALDI-TOF mass spectrum of the aforementioned complex showing the bimodal distribution, due to different populations of guest species [38].

obtain a partial structure confirming capsule formation, Figure 14.14A). Analysis using MALDI-TOF MS on the copper nanocapsule precipitates displayed a broad bimodal distribution for each material [38], where the main peaks from either end of the distribution display a consistent mass difference of 633–635 atomic mass units, thereby reflecting the mass difference between a full (empty copper capsule + either 20 MeOH, 35 H_2O or any combination of both) and an empty copper capsule (i.e. one in which there are no apical ligands on the metal centers and no guest species) as shown in Figure 14.14B.

As described for the third generation capsules, ethyl acetate was found to be an excellent solvent for the growth of single crystals of the *C*-alkylpyrogallol[4]arenes (where alkyl chains range from butyl to undecyl) [21,22]. With longer chains at the lower rim, dodecyl and tridecyl, crystallization from this solvent afforded bilayer structures, indicating that van der Waals forces overcome capsule formation in the solid state at this point. Despite this, a combination of a methanolic solution of these pyrogallol[4]arenes and excess $Cu(NO_3)_2$ in methanol also resulted in the instantaneous formation of a brown precipitate, which was confirmed by MALDI-TOF MS to be the relevant copper nanocapsules. This experiment demonstrated that templation by the hydrogen-bonded hexamers was not a requirement and actually may not play any role whatsoever in the formation of the copper nanocapsule analogues [38].

This was given further credence by reacting a 1:1 mixture of PgC_6 and PgC_{11} as previously described with excess $Cu(NO_3)_2$, again resulting in the instantaneous formation of a brown precipitate [38]. Avram and Cohen had previously reported that there was a degree of self-association among mixtures of *C*-alkylpyrogallol[4]arenes over an initial 24-h period, after which time a mixed formation of hexameric hydrogen-bonded capsules resulted [39]. The results from our MALDI-TOF MS experiments, however, displayed an instantaneous formation of a statistical mixture of all permutations of metal–organic nanocapsules that could possibly result from

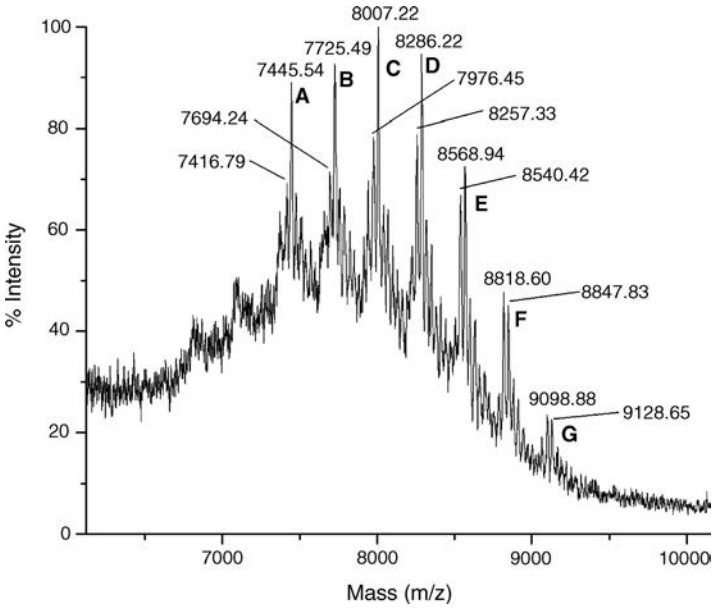

Figure 14.15 MALDI-TOF MS displaying statistical permutations of metal–organic nanocapsules formed from the reaction of copper nitrate and a 1:1 mixture of *C*-hexyl- and undecylpyrogallol [4]arenes. Peaks A–G reflect PgC_6:PgC_{11} ratios of 6:0, 5:1, 4:2, 3:3, 2:4, 1:5 and 0:6, respectively [38].

the mixture of two pyrogallol[4]arenes, as shown in Figure 14.15 [38]. This suggests a very rapid and indiscriminate reaction of the Cu^{2+} ions with the pyrogallol[4]arenes, thereby showing no inclination to fit within a preordered templation sequence of the hydrogen-bonded hexameric nanocapsules.

In our exploration of other metals that may react to form similar metal–organic nanostructures based on hydrogen-bonded assemblies, gallium nitrate was considered an interesting alternative. The reaction of *C*-propylpyrogallol[4]arene with 4 equivalents of $Ga(NO_3)_3$ in acetone–water gave single crystals over a matter of hours. Structural analysis revealed the metal–organic capsule $[Ga_{12}(H_{20})_{24}(C_{40}H_{40}O_{12})_6(acetone)_8(H_{20})_6]$ which was assembled from a total of 18 components, i.e. six cavitands and 12 Ga^{3+} ions, as opposed to the expected 24 metal ions in the copper-seamed capsules (Figure 14.16) [40].

With the formation of 48 equatorial Ga–O bonds and the concomitant replacement of 36 protons, there remains a further 36 phenoxy protons which participate in hydrogen bonding, 20 of which are intramolecular and the remaining 16 interact with H_2O in hydrogen bonds that seal up potential surface voids. The vast difference in the hydrogen bonding, induced by the metal centers, results in the formation of a distorted "rugby ball"-like structure, as shown in Figure 14.16. The axial positions of the Ga^{3+} ions are coordinated with 24 H_2O molecules, 12 of which are ligated from the capsules innards, resulting in the ordering of the nanocapsule interior, which eight acetone and 20 water molecules, six of which are non-coordinated waters

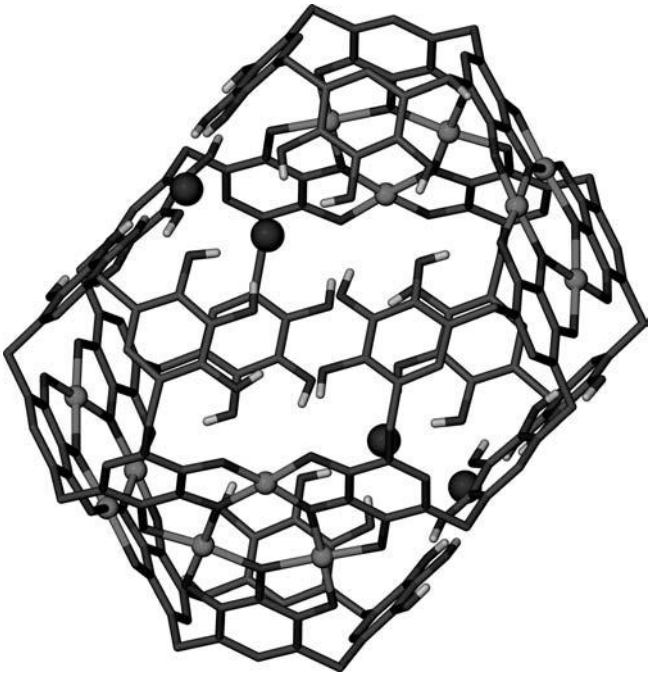

Figure 14.16 The metal–organic nanocapsule formed by reaction of *C*-propylpyrogallol[4]arene with gallium nitrate. Note the distorted "rugby ball"-like shape of the nanocapsule in addition to the presence of surface water molecules (shown as dark spheres) [40].

involved in two hydrogen-bonded chains $(H_2O)_5$. A variety of other *C*-alkylpyrogallol [4]arenes have been utilized for capsule formation with Ga^{3+} ions from an acetonitrile–water solvent system [41]. Although in some cases the crystals proved to be unstable to solvent loss once removed from the mother liquor, a suitably stable single crystal for X-ray diffraction formed from *C*-pentylpyrogallol[4]arene, but in general the interior of these capsules is less well ordered compared with the acetone–water system.

Given the instantaneous nature of the formation of copper pyrogallol[4]arene nanocapsules, we investigated the possibility of exploiting the voids found in the surfaces of the gallium nanocapsules, as shown in Figure 14.16. Gallium *C*-proylpyrogallol[4]arene capsules were suspended in an acetone–methanol solution and addition of methanolic $Cu(NO_3)_2$ resulted in immediate dissolution of the crystals and a color change from blue–green to red–brown, but notably no precipitate formation. Slow evaporation of the solution gave single red crystals that were analyzed using a synchrotron radiation source, affording the expected "stitched up" nanocapsule (Figure 14.17) [38].

The structure could be solved using either copper or gallium (which is not unsurprising given their proximity in the Periodic Table) and inductively coupled plasma (ICP) analysis was employed to determine the Cu:Ga ratio in the sample.

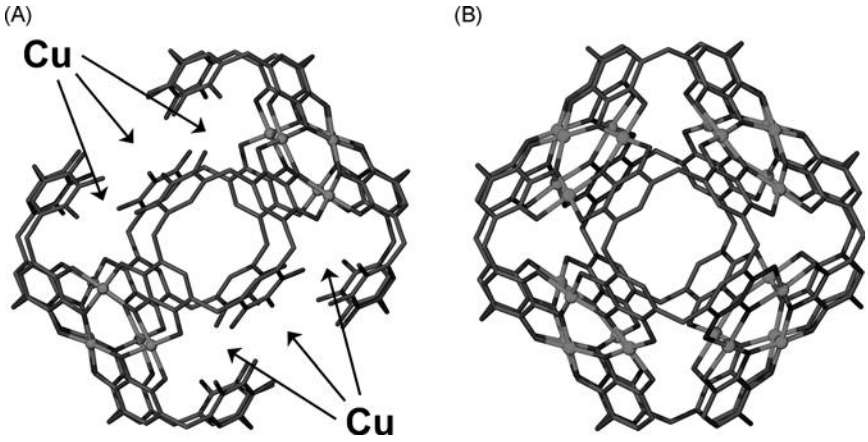

Figure 14.17 (A) The theoretical open binding sites in the gallium nanocapsule shown in Figure 14.16 that are available to copper centers (surface water molecules omitted for clarity). (B) The crystal structure of the mixed metal nanocapsule formed after copper addition [38].

Surprisingly, this was found to be 2:1 (i.e. 16:8 in a nanocapsule), indicating that not only had the Cu centers seamed the surface voids, but also that they expelled and replaced four Ga^{2+} ions, presumably one from each preformed gallium nanocapsule "face". We postulate that the copper exerts a structural correction to the distorted gallium nanocapsule, thus resulting in the expulsion of one gallium center from each array and its replacement by a $Cu^{2}+$ ion [38].

In a similar approach to that used to form the copper nanocapsules, i.e. using hydrogen-bonded arrangements as theoretical blue prints, a search of the Cambridge Structural Database (CSD) revealed a dimeric *C*-propylpyrogallol[4]arene capsule, reported by Rebek and coworkers [42], which is asymmetric and which possesses a complex polar belt of hydrogen bonds that appeared suitable for metal retro-insertion. Given that a square-planar or octahedral metal center would preclude complex formation with this capsule based on the angles associated with the oxygen atoms of the macrocycles, we investigated zinc (amongst other suitable metals) as a potential complexing agent.

Initial studies with this system found that combination of *C*-propylpyrogallol[4]arene in pyridine (color change from clear to dark) with 4 equivalents of $Zn(NO_3)_2$ resulted in the growth of colored single crystals of the complex [Zn_8(*C*-propylpyrogallol[4]arene)$_2$(pyridine)$_8$ ⊂ pyridine] over time (Figure 14.18A) [43]. Characterization by X-ray diffraction and MALDI-TOF MS showed a dimeric metal organic capsule composed of 10 components, two cavitands which have had 16 of their 24 protons replaced by the concomitant coordination of eight Zn^{2+} ions, an encapsulated guest pyridine molecule (disordered due to molecular rotation) and eight axial solvent ligands. Each of the zinc centers is pentacoordinate with four phenoxy groups (arranged in a distorted plane) and an axial pyridine, all of which affords a distorted square-pyramidal configuration (Figure 14.18B).

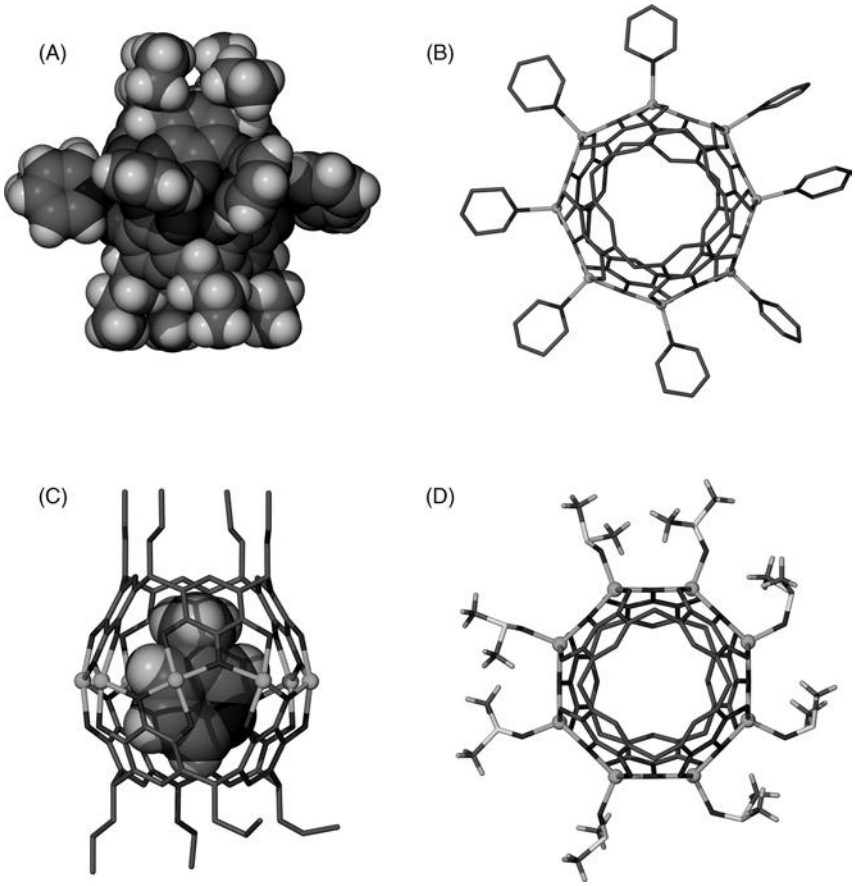

Figure 14.18 Octametallated dimeric capsules formed by reaction of zinc pyridine complexes with *C*-propylpyrogallol[4]arene. (A) The pyridine-containing capsule in space filling representation. (B) Alternative view of (A) showing pyridine ligation at zinc centers [43]. (C) Space filling model of encapsulated 3-methylpyridine. (D) DMSO ligation at zinc centers demonstrating ligand exchange [44].

As pyridine appeared to play a crucial role in the dimeric metal-seamed capsule formation, the complex $[Zn(NO_3)_2(pyridine)_3]$ was dissolved in MeOH and mixed with a methanolic solution of *C*-propylpyrogallol[4]arene, giving an instantaneous yellow precipitate which was analyzed and confirmed to be the target metal–organic dimer. This concomitantly allowed for facile variation of guest species and metal ligands including 3-picoline [44], 4-picoline, 4-ethylpyridine and 1-methylimidazole [45]. For purposes of crystallization, the most suitable solvent was found to be DMSO, which also readily exchanged with the heterocycle as a ligand, with complete exchange being achieved via dialysis (Figure 14.18 C and D) [44].

Both ^{1}H and ^{13}C NMR analysis demonstrated the influences of a "tight" or confined space on the guest, a feature that was immediately noticeable by significant

upfield shifts for the guest relative to those of the free molecule, a feature that has also been observed for carcerands [46]. For encapsulated 3-picoline, the methyl group experiences a $\Delta\delta$ greater than 4 ppm, reflecting the strong CH$\cdots\pi$ interaction between host and guest, while the remaining $\Delta\delta$ values for the guests aromatic protons reflect their equatorial positioning within the dimeric capsule, although these are still significant [44]. This correlates with the crystal structure in which the 3-picoline methyl group is shown to be clearly positioned in close proximity to the arene moiety of the capsule (Figure 14.18).

It was observed that upon ligand replacement of DMSO, the ^{1}H NMR upfield shift for the encapsulated guest was sensitive to change. This is most likely a consequence of the electropositive metal centers supplementing for the loss of electron density by drawing from the aryl rings, thus affecting host–guest interactions. A series of titration studies were initiated by the reintroduction of free 3-picoline to a DMSO-d_6 solution of the DMSO-ligated metal–organic dimer, where the guest shows a downfield signal shift by each of its protons (Figure 14.19). This reflects a change in electron density distribution throughout the capsule, which of course would have an influence on the guest's mobility and CH$\cdots\pi$ interactions.

MALDI-TOF MS analysis on the [Zn_8(*C*-propylpyrogallol[4]arene)$_2$(pyridine)$_8$ $\subset$ pyridine] complex revealed two significant peaks corresponding to the zinc dimeric capsules that are either occupied or vacuous. Notably, this is the third capsular system in which we have recently observed significant void space, $\sim$ 80 Å^3 in the fourth generation capsules and $\sim$1500 and $\sim$140 Å^3 for the copper and zinc capsules described in this section. We are now looking at exploiting these large voids for

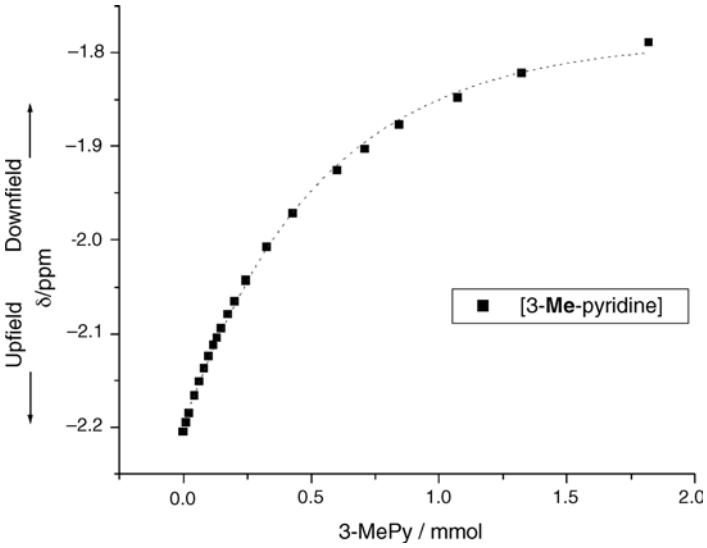

Figure 14.19 Titration plot of ligand concentration versus methyl shift of encapsulated 3-picoline guest, showing an increase in δ owing to the exchange of DMSO for electron donating 3-picoline ligands on zinc centers [44].

molecular entrapment that may be deemed indiscriminate within steric considerations for example.

14.7
Sixth Generation Nanocapsules

The largest closed capsule structurally characterized thus far is the hexamer **3** with an enclosed volume of ~1500 Å^3 [25]. It is anticipated that it may well be possible to enclose (without molecule-sized pores) up to ~2500 Å^3 of chemical space. To enclose completely even more space, one will most likely need larger synthons given that the bulding blocks we have described are highly self-complementary and routinely form those assemblies outlined above. Our first attempts in the area of larger capsules have involved using alkyl chains of varying length and functionality radiating from the hydrogen-bonded and metal–organic nanocapsules. As mentioned above, pyrogallol [4]arenes have been shown to crystallize in either bilayer or hexameric nanocapsule motifs, depending on the crystallization solvent employed [19,21–24,30,33,38]. Although this is the case, little was known of the aggregation and supermolecular assembly of these solution stable entities. To our surprise, a wide variety of packing motifs have been observed for hexameric nanocapsules in the solid state [21,22,24]. Of particular interest is the long-chain motif shown in Figure 14.20 [22]. The alkyl chains effectively pack only in two dimensions, leaving the third dimension free for solvent inclusion. This provided the clue that such simple capsules might indeed form the building blocks for even larger structures. We recently shed light on this behavior through the use of dynamic light scattering (DLS), transmission and scanning electron microscopy (TEM and SEM, respectively) and atomic force microscopy (AFM) techniques to find very large structures/aggregates that are ~80–500 nm in size/diameter (Figure 14.21) [47].

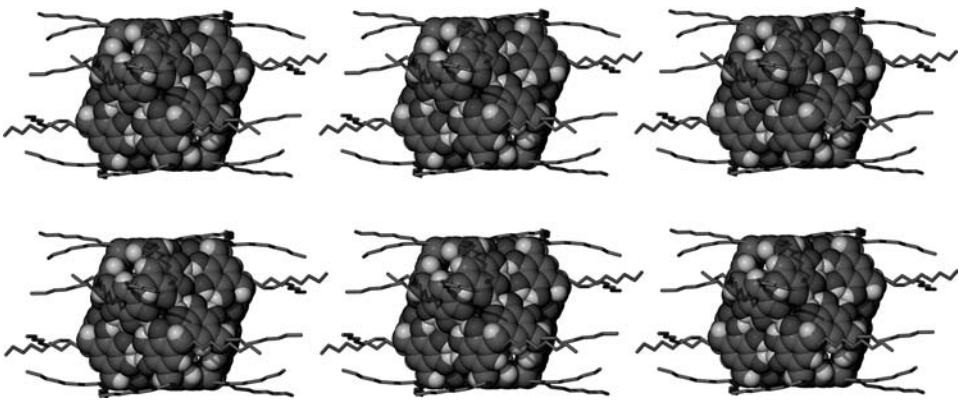

Figure 14.20 Packing of *C*-nonylpyrogallol[4]arene nanocapsules. Note that the alkyl chains pack in a two-dimensional like arrangement, exposing hydrogen-bonded faces of the nanocapsules in the third dimension [22].

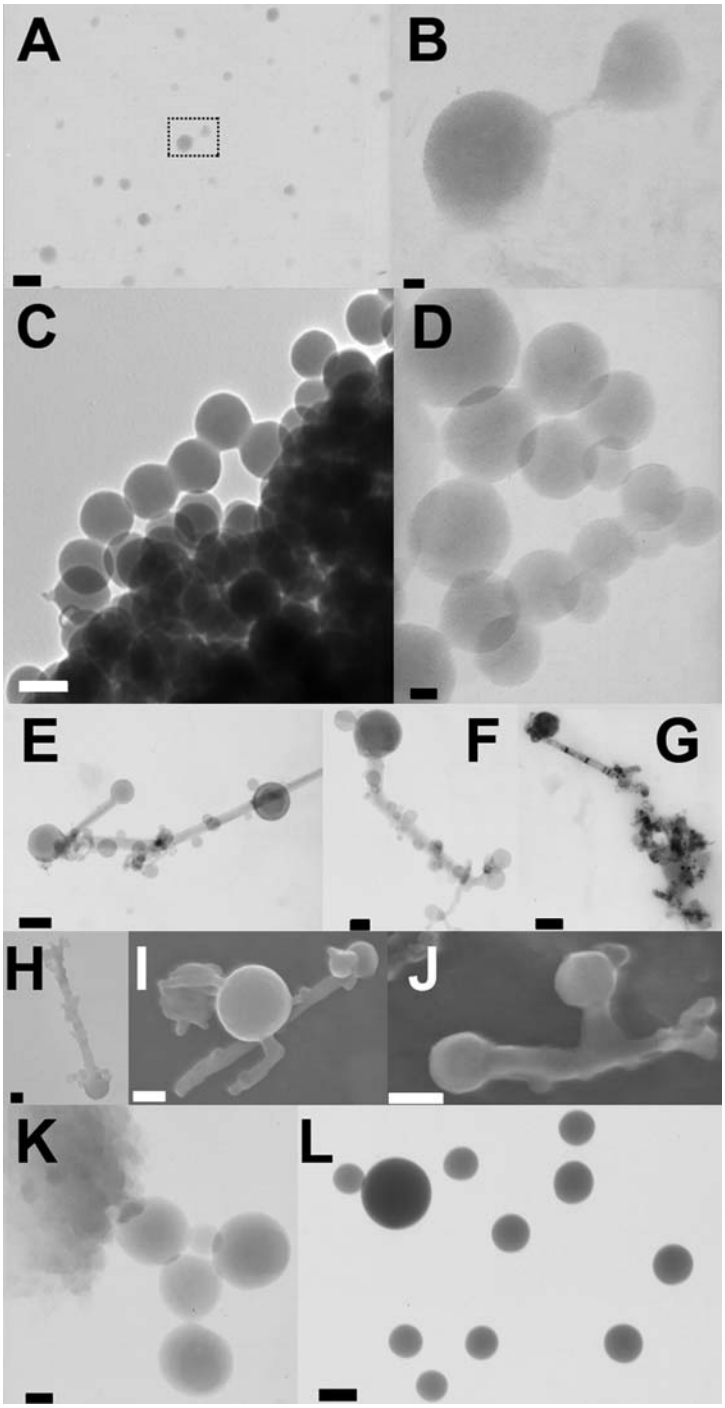

Figure 14.21 Various TEM (A–G, K, L) and SEM (H–J) images showing the large spherical and tubular aggregates formed from hydrogen-bonded and metal–organic nanocapsules [47].

Through the use of DLS, the large supermolecular aggregates were observed for different hydrogen-bonded pyrogallol[4]arene hexamers under dilute conditions (typical concentration $\sim 10^{-3}$ M). Given the stability and recurring nature of the aggregates in solvents other than water, TEM, SEM and AFM were further used to examine the particles formed, the results of which were unexpected [47]. Evaporation of a $\sim 10^{-4}$ M acetone solution of the hydrogen-bonded *C*-isobutylpyrogallol[4]arene hexamer under ambient conditions afforded large, spherical aggregates that were observed by TEM (Figure 14.21A). The aggregates were found to be spherical, of uniform shape and with wide-ranging diameters (92 ± 42 nm) when formed from acetone solutions. Furthermore, the spherical aggregates were (on occasion) found to be linked by interesting tubular architectures as shown in Figure 14.21B. The rate of evaporation was found to play a role in aggregate formation. By employing higher boiling solvents in sample preparation, the number of observed aggregates was reduced and this process also typically led to alternative crystal growth as observed via TEM studies. Similar observations were seen for other solvent systems such as methylene chloride, acetonitrile and chloroform with the visualization of stacked aggregates in the last two systems (Figure 14.21C and D). AFM further corroborated the presence of large spherical aggregates, with similar-sized particles being observed using this additional technique.

Given that lipophilic calix[4]arenes have been shown to form solid lipid nanoparticles that collapse upon solvent removal [48], coupled with the fact that pyrogallol[4]arenes can form such bilayer arrangements [38], it was necessary to determine whether the submicron aggregates were formed from hydrogen-bonded layers or hexamers. In order to probe this, analogous metal-coordinated capsules (fifth generation gallium hexamers that are incapable of disassembly in the solvent systems employed) were studied using TEM. The results of these studies on this system were spherical aggregates with dimensions comparable to those of the hydrogen-bonded analogues. The images produced were significantly darker, presumably due to the high content of gallium in the resultant superstructures (Figure 14.21K and L). This compelling evidence suggests that the spherical aggregates *are* indeed composed of many discrete hexamer building blocks (or hydrogen-bonded analogues) and are *not* a bilayer-related motif.

In general, the tubular connectors were of smaller diameter than the spherical aggregates, which were often found at the tubule ends. These tubules were found to exist in both smooth and rugged morphologies with lengths approaching 1 μm (Figure 14.21E–J). Examination of the smooth and rugged tubes using TEM and SEM, respectively, showed hemispherical swellings that appeared to be spherical aggregates budding from the tubular architectures (Figure 14.21E, F, H–J). These budding aggregates are spread randomly across the length of the tubes and are of comparable diameter. When observing the freshly deposited submicron spheres and tubes using TEM, bands of dark material could be seen to travel the length of the tubular structures (Figure 14.21G). Additional observations showed that spheres connected to tubes had electron dark regions. Upon exposure to the beam, this region diffused from the sphere along the tube as a dark band. Such dark band movement may be attributable to the energy of the electron beam that could cause regional heating, thereby forcing the trapped solvent to undergo translation due to a

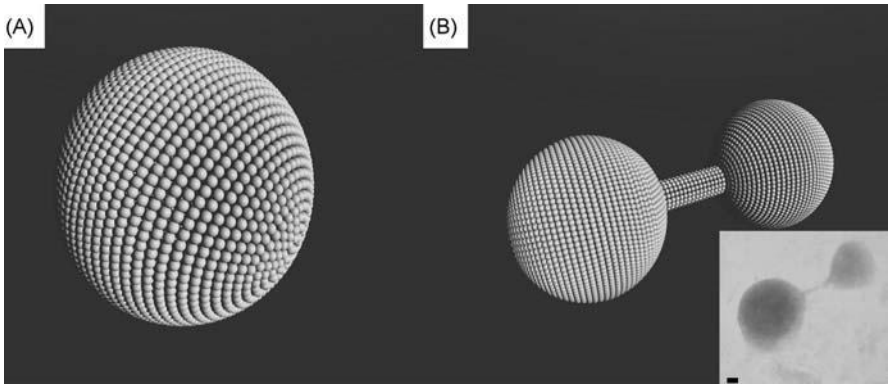

Figure 14.22 Schematic of many nanocapsules arranged into spherical and tubular aggregates (see inset experimental figure) [47].

temperature gradient. This phenomenon was only observed on freshly prepared TEM samples that had residual solvent present, and samples re-examined after a number of days showed no sign of such band movement.

By conducting *in situ* experiments with crystals of pyrogallol[4]arene hexamers with the electron beam (TEM), we were able to discover a direct route to the tubular and spherical aggregates. Using this method, we discovered that as the TEM beam is entrained upon these single crystals, spherical and at times tubular aggregates would also form as the crystalline material decomposes.

Figure 14.22 provides a model of the submicron sphere and tube based on the association of pyrogallol[4]arene nanocapsules. By altering the length of the alkyl chains radiating from the lower rims of the pyrogallol[4]arenes, we aim to introduce further control over the aggregation properties of these nanocapsules to afford larger or desirable nanoparticles for future application.

14.8
From Spheres to Tubes

Spheres and tubes are intimately related, an excellent example of which is fullerene C_{60} and single-walled carbon nanotubes [49,50]. Indeed, these two materials have attracted much interest and it is surprising that much less effort has been invested in developing the synthesis of alternative multicomponent organic nanospheres and tubules. Only a limited number of purely organic nanotubes that have large internal channel volumes have been reported to date, the majority of which are formed through the self-assembly of cyclic oligomers composed of peptides [51], ureas [52] or carbohydrates [53]. However, an important example to be highlighted is the back-to-back solid-state assembly of calix[4]hydroquinone, resulting in a multicomponent organic nanotube [54] which is stabilized by π-stacking interactions between adjacent calixarenes and which was used to form ultrathin silver nanowires.

As mentioned in the section on second generation capsules, it was shown that deviation from the typical anti-parallel bilayer arrangement of *p*-sulfonatocalix[4]arene (Figure 14.2) to form a nanoscale icosahedral arrangement (Figure 14.3) could be achieved through variation of the stoichiometries of the calixarene, pyridine *N*-oxide and metal cation [15]. In addition to forming a near-spheroidal icosahedral arrangement, the *C*-shaped dimer used to form this assembly can also be tailored into nanotubules which contain additional PNO as a spacer molecule. The diameter of these tubules is similar to that of the icosahedral arrangement and the core is composed of hydrated sodium and lanthanum cations.

More recently, and in relation to the first generation of capsules, Rissanen and co-workers showed that *C*-methylresorcin[4]arene can be co-crystallized such that

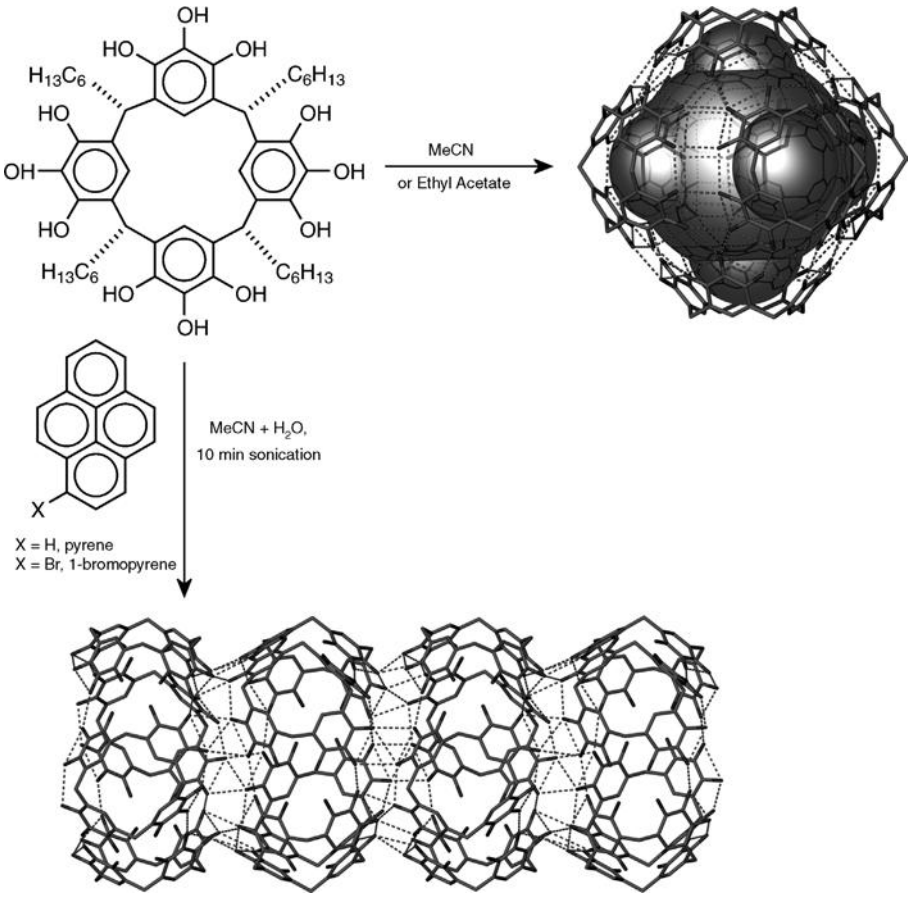

Figure 14.23 The conditions required to form either nanocapsules or nanotubular arrays of *C*-hexylpyrogallol[4]arene. In the latter, pyrene or 1-bromopyrene acts as a type of molecular glue on the exterior of the nanotubular assembly, interacting through many van der Waals interactions [56].

the molecule forms a back-to-back nanotubular arrangement, which contains a small core that is capable of solvent exchange [55]. This is the second example in which a molecule used to form a nanocapsule can be manipulated into a nanotubular array, although in this case the orientation of the host molecule is reversed, i.e. back-to-back rather than face-to-face as in **1**, and differs from the *p*-sulfonatocalix[4]arene examples in which the orientation is the same (both are parallel packing).

We have recently reported the third such example of nanocapsule to nanotube conversion, which is also the second example of packing retention. *C*-Hexylpyrogallol [4]arene, when co-crystallized in the presence of pyrene or 1-bromopyrene from a hot sonicated acetonitrile–water solution and followed by cooling and slow evaporation, forms large single crystals that were structurally analyzed to be pyrogallol[4] arene-based nanotubes. The pyrogallol[4]arene in the nanotube arrays form cyclic or disk-like tetramers through hydrogen bonds. These tetramers are found to link together in a tubular fashion through additional hydrogen-bond interactions, with each tetramer being rotated by approximately 45° relative to an axis running down the nanotube array, all of which shrouds alternating microenvironments of water and acetonitrile that form numerous hydrogen bonds on the interior [56]. In relation to the third generation capsules based on pyrogallol[4]arenes, these tetramers have a diameter nearly identical with that of the corresponding *C*-hexylpyrogallol[4]arene nanocapsule when crystallized from acetonitrile, thereby demonstrating structural retention (Figure 14.23). The pyrene or 1-bromopyrene co-crystallizing species are crucial for nanotube formation, as they interact through numerous van der Waals forces on the exterior of the assemblies behaving like a type of "molecular glue".

It is apparent from these series of results that when a near-spherical calixarene-based nanocapsule is obtained, there should be a strong possibility of isolating the related nanotubular array in either a similar or reversed packing mode. The same should also be true *vice versa*, although this may require a degree of experimentation to achieve.

14.9 Conclusions

We have described a number of generations of organic nanocapsules, and also metal–organic analogues, and have shown that rational design often leads to elegant nanostructures. We have demonstrated the encapsulation of probe molecules in stable hydrogen-bonded hexameric nanocapsules and significant advancements have been made in the area of metal–organic capsules using non-covalent assemblies as theoretical templates. This has been a particularly fruitful approach and the ability to sense ligands on metal centers, while also trapping chosen chemical species indiscriminately (using copper pyrogallol[4]arene nanocapsules, for example) is a very interesting opportunity to explore further this rapidly expanding and burgeoning field of capsule chemistry. It may also be true that a series of metal–organic nanotubular arrays will also be realized, but it is likely that only after significant

control is gained over structures such as those described in this chapter will function follow levels of rational design. Some of the above strategies may perhaps be applicable to other systems that contain similar functional properties to some of the macrocycles described herein.

Acknowledgments

We would like to thank all those involved with this work to date, with particular thanks to Professor L. J. Barbour, Dr. Agoston Jerga and Dr. Gareth Cave.

References

1 Collet, A. (1987) *Tetrahedron*, **43**, 5725.
2 Cram, D.J., Choi, H.-J., Bryant, J.A. and Knobler, C.B. (1992) *J. Am. Chem. Soc.*, **114**, 7748.
3 Conn, M.M. and Rebek, J. Jr. (1997) *Chem. Rev.*, **97**, 1647.
4 Rose, K.N., Barbour, L.J., Orr, G.W. and Atwood, J.L. (1998) *Chem. Commun.*, 407.
5 Murayama, K and Aoki, K. (1998) *Chem. Commun.*, 607.
6 Shivanyuk, A., Paulus, E. and Böhmer, V. (1999) *Angew. Chem. Int. Ed.*, **38**, 2906.
7 González, J.J., Ferdani, R., Albertini, E., Blasco, J.M., Arduini, A., Pochini, A., Prados, P. and de Mendoza, J. (2000) *Chem. Eur. J.*, **6**, 73.
8 Shivanyuk, A., Rissanen, K. and Kolehmainen, E. (2000) *Chem. Commun.*, 1107.
9 Atwood, J.L. and Szumna, A. (2002) *J. Am. Chem. Soc.*, **124**, 10646; Atwood, J.L. and Szumna, A. (2003) *Chem. Commun.*, 940.
10 MacGillivray, L.R. and Atwood, J.L. (1997) *Nature*, **389**, 469.
11 Aoyama, Y., Tanaka, Y. and Sugahara, S. (1989) *J. Am. Chem. Soc.*, **111**, 5397.
12 Evan-Salem, T., Baruch, I., Avram, L., Cohen, Y., Palmer, L.C. and Rebek, J. Jr. (2006) *Proc. Natl. Acad. Sci. USA*, **103**, 12296.
13 Avram, L. and Cohen, Y. (2003) *Org. Lett.*, **5**, 1099.
14 MacGillivray, L.R. and Atwood, J.L. (1999) *Angew. Chem. Int. Ed.*, **38**, 1018.
15 Orr, G.W., Barbour, L.J. and Atwood, J.L. (1999) *Science*, **285**, 1049.
16 Atwood, J.L., Hamada, F., Robinson, K.D., Orr, G.W. and Vincent, R.L. (1991) *Nature*, **349**, 683; Coleman, A.W., Bott, S.D., Morley, S.D., Means, C.M., Robinson, K.D., Zhang, H. and Atwood, J.L. (1988) *Angew. Chem. Int. Ed. Engl.*, **100**, 1412; Atwood, J.L., Coleman, A.W., Zhang, H., and Bott, S.D. (1989) *J. Inclusion Phenom. Mol. Recognit. Chem.*, **7**, 203.
17 Atwood, J.L., Barbour, L.J., Dalgarno, S.J., Hardie, M.J., Raston, C.L. and Webb, H.R. (2004) *J. Am. Chem. Soc.*, **126**, 13170.
18 Dalgarno, S.J., Atwood, J.L. and Raston, C.L. (2006) *Chem. Commun.*, 4567.
19 Gerkensmeier, T., Iwanek, W., Agena, C., Frohlich, R., Kotila, S., Nather, C. and Mattay, J. (1999) *Eur. J. Org. Chem.*, 2257.
20 Meissner, R.S., Rebek, J. Jr. and de Mendoza, J. (1995) *Science*, **270**, 1485.
21 Cave, G.W.V., Antesberger, J., McKinlay, R.M. and Atwood, J.L. (2004) *Angew. Chem. Int. Ed.*, **43**, 5263.
22 Cave, G.W.V., Dalgarno, S.J., Antesberger, J., Ferrarelli, M., McKinlay, R.M. and Atwood, J.L. (2007) Supramol. Chem., In press.
23 Dalgarno, S.J., Power, N.P., Antesberger, J., McKinlay, R.M. and Atwood, J.L. (2006) *Chem. Commun.*, 3803.
24 Dalgarno, S.J. Antesberger, J. McKinlay, R.M. Atwood, J.L. (2007) Chem. Eur. J., **13**, 8248.

25 Atwood, J.L., Barbour, L.J. and Jerga, A. (2001) *Chem. Commun.*, 2376.

26 Shivanyuk, A. and Rebek, J. Jr. (2003) *J. Am. Chem. Soc.*.**125**, 3432; Shivanyuk, A. and Rebek, J. Jr. (2001) *Proc. Natll. Acad. Sci. USA*, **98**, 7662; Yamanaka, M., Shivanyuk, A. and Rebek, J. Jr. (2004) *J. Am. Chem. Soc.*, **126**, 2939; Palmer, L.C., Shivanyuk, A., Yamanaka, A. and Rebek, J. Jr. (2005) *Chem. Commun.*, 857.

27 Avram, L. and Cohen, Y. (2002) *J. Am. Chem. Soc.*, **124**, 15148; Avram, L. and Cohen, Y. (2002) *Org. Lett.*, **4**, 4365; Avram, L. and Cohen, Y. (2004) *J. Am. Chem. Soc.*, **126**, 11556.

28 Caspar, D. and Klug, A. (1962) *Cold Spring Harbor Symp. Quant. Biol.*, **27**, 1; Casjens, S. (1995) *in Virus Structure and Assembly*, Jones and Bartlett, Boston.

29 Rudkevich, D.M. and Rebek, J. Jr. (1999) *Eur. J. Org. Chem.*, 1991.

30 Dalgarno, S.J., Tucker, S.A., Bassil, D.B. and Atwood, J.L. (2005) *Science*, **309**, 2073.

31 Dalgarno, S.J., Szabo, T., Siavosh-Haghighi, A., Deakyne, C., Adams, J.E. and Atwood, J.L. (2007) *J. Am. Chem. Soc.*, submitted.

32 Unpublished results, in preparation.

33 Dalgarno, S.J., Bassil, D.B., Tucker, S.A. and Atwood, J.L. (2006) *Angew. Chem. Int. Ed.*, **45**, 7019.

34 Bassil, D.B., Dalgarno, S.J., Cave, G.W.V., Tucker, S.A. and Atwood, J.L. (2007) *J. Phys. Chem. B*, **111**, 9088.

35 Atwood, J.L., Barbour, L.J. and Jerga, A. (2002) *Proc. Natl. Acad. Sci. USA*, **99**, 4837.

36 Fuchs, R., Habermann, N. and Klüfers, P. (1993) *Angew. Chem. Int. Ed. Engl.*, **32**, 852.

37 McKinlay, R.M., Cave, G.W.V. and Atwood, J.L. (2005) *Proc. Natl. Acad. Sci. USA*, **102**, 5944.

38 Dalgarno, S.J., Power, N.P., Warren, J. and Atwood, J.L. (2007) *Angew. Chem. Int. Ed.*, submitted.

39 Avram, L. and Cohen, Y. (2004) *J. Am. Chem. Soc.*, **126**, 11556.

40 McKinlay, R.M., Thallapally, P.K., Cave, G.W.V. and Atwood, J.L. (2005) *Angew. Chem. Int. Ed.*, **44**, 5733.

41 McKinlay, R.M., Thallapally, P.K. and Atwood, J.L. (2006) *Chem. Commun.*, 2956.

42 Shivanyuk, A., Friese, J.C., Doring, S. and Rebek, J. Jr. (2003) *J. Org. Chem.*, **68**, 6489.

43 Power, N.P., Dalgarno, S.J. and Atwood, J.L. (2007) *New J. Chem.*, **31**, 17.

44 Power, N.P., Dalgarno, S.J. and Atwood, J.L. *Angew. Chem. Intl. Ed*, **46**, 8601.

45 Unpublished results, in preparation.

46 Chapman, R.G. and Sherman, J.C. (2000) *J. Org. Chem.*, **65**, 513.

47 Heaven, M.W., McKinlay, R.M., Antesberger, J., Dalgarno, S.J., Thallapally, P.K. and Atwood, J.L. (2006) *Angew. Chem. Int. Ed.*, **45**, 6221.

48 Shahgaldian, P., Da Silva, E., Coleman, A.W., Rather, B. and Zawarotko, M.J. (2003) *Int. J. Pharm.*, **253**, 23, and references therein.

49 Kroto, H.W., Heath, J.R., O'Brien, S.C., Curl, R.F. and Smalley, R.E. (1985) *Nature*, **318**, 162.

50 Ramirez, A.P., Haddon, R.C., Zhou, O., Fleming, R.M., Zhang, J., McClure, S.M. and Smalley, R.E. (1994) *Science*, **265**, 84.

51 Ghadiri, M.R., Granja, J.R., Milligan, R.A., McRee, D.E. and Khazanovich, N. (1993) *Nature*, **366**, 324; Hartgerink, J.D., Granja, J.R., Milligan, R.A. and Ghadiri, M.R. (1996) *J. Am. Chem. Soc.*, **118**, 43.

52 Semetey, V., Didierjean, C., Briand, J.-P., Aubry, A. and Guichard, G. (2002) *Angew. Chem. Int. Ed.*, **41**, 1895.

53 Gattuso, G., Menzer, S., Nepogodiev, S.A., Stoddart, J.F. and Williams, D.J. (1997) *Angew. Chem. Int. Ed. Engl.*, **36**, 1451.

54 Hong, B.H., Bae, S.C., Lee, C.-W., Jeong, S. and Kim, K.S. (2001) *Science*, **294**, 348.

55 Mansikkamäki, H., Nissinen, M. and Rissanen, K. (2004) *Angew. Chem. Int. Ed.*, **43**, 1243.

56 Dalgarno, S.J., Cave, G.W.V. and Atwood, J.L. (2006) *Angew. Chem. Int. Ed.*, **45**, 570.